Study of Electrochemical Impedance Spectroscopy and Cyclic Voltammetry of Commercial Lithium-ion Battery at Elevated Temperature

This thesis is submitted to the Department of Mechanical Engineering of Chittagong University of Engineering & Technology as a partial fulfillment of requirement for the degree of

MASTER OF SCIENCE IN MECHANICAL ENGINEERING

Submitted By

Aoyon Paul

Student ID: 21MME031P

Supervised by

Professor Dr. Md. Arafat Rahman

Department of Mechanical Engineering

Department of Mechanical Engineering

Chittagong University of Engineering &Technology

Approval

The thesis titled "Study of Electrochemical Impedance Spectroscopy and Cyclic Voltammetry of Commercial Lithium-ion Battery at Elevated Temperature" submitted by Aoyon Paul, ID- 21MME031P, Session: 2021-2022 has been accepted as satisfactory in partial fulfillment of the requirement for the degree of Master of Science (M.Sc.) in Mechanical Engineering dated on 15th December 2024.

Board of Examiners

1.	**Dr. Md. Arafat Rahman** Professor, Department of Mechanical Engineering, CUET	**Chairman** **(Supervisor)**
2.	**Head** Department of Mechanical Engineering, CUET	**Member** **(Ex-Officio)**
3.	**Dr. Sheikh Muhammad Humayun Kabir** Professor, Department of Mechanical Engineering, CUET	**Member**
4.	**Dr. Mohammad Mizanur Rahman** Professor, Department of Mechanical Engineering, CUET	**Member**
5.	**Dr. Md. Saiful Islam** Assistant Professor, Department of Nanomaterials and Ceramic Engineering, BUET	**Member** **(External)**

List of Publications

Parts of this M. Sc. Engineering thesis have already been published in referred scientific journals as follows:

- **Aoyon Paul**, Md Arafat Rahman, Nirjhor Barua, "**Study of temperature cycling of commercial rechargeable lithium-ion batteries**", Future Sustainability, 2023: https://doi.org/10.55670/fpll.fusus.1.1.3, Vol. 1 No. 1, Published: 15 Nov 2023.

- Konok Chandra Bhowmik, Md Arafat Rahman, Md Muktadir Billah, Aoyon Paul, "From Lithium-Ion to Sodium-Ion Batteries for Sustainable Energy Storage: A Comprehensive Review on Recent Research Advancements and Perspectives". The Chemical Record, 2024; https://doi.org/10.1002/tcr.202400176, Published: 20 Nov 2024.

- Aoyon Paul, Md Arafat Rahman, Konok Chandra Bhowmik, "Measurement of Internal Resistance of Lithium-ion Batteries by Electrochemical Impedance Spectroscopy: A Critical Review", Journal Under Review in Trends in Science.

Declaration

I hereby declare that this thesis represents my work which has been done after registration for the degree of M.Sc. in Mechanical Engineering at CUET and has not been previously included in a thesis or dissertation submitted to this or any other institution for a degree, diploma, or other qualification.

Name: Aoyon Paul

Student ID: 21MME031P

Date: -…..……..

Acknowledgment

At the very beginning, I would like to praise the Almighty God who has given me the ability to complete this report and my heartfelt appreciation goes out to everyone who helped me finish this thesis.

Above all, I owe a debt of gratitude to my supervisor Professor Dr. Md. Arafat Rahman, Department of Mechanical Engineering, CUET, for his essential advice during the research process. His knowledge, tolerance, and insightful feedback were invaluable in helping to shape this thesis.

I express my sincere gratitude to the members of my thesis committee, namely Dr. Mohammad Mizanur Rahman, Professor, Head of the ME Department at CUET, Dr. Sheikh Muhammad Humayun Kabir, Professor, Department of Mechanical Engineering, CUET, and Dr. Md. Saiful Islam, Assistant Professor, Department of Nanomaterials and Ceramic Engineering, BUET, for their invaluable time, expertise, and critical assessment of this work.

I extend my sincere appreciation to the faculty and staff of CUET for providing a stimulating academic environment and access to valuable resources that facilitated my research endeavors.

Dedication

This thesis is dedicated to my parents and my younger sister for their endless supports, love and sacrifices.

Abstract

Li-ion batteries have become essential in everything from consumer electronics to renewable energy systems. However, they also suffer from some key performance and safety challenges, mainly arising at high temperatures. In general, high temperatures increase the kinetics of various degradation processes such as gas production, lithium plating, and electrolyte breakdown, resulting in capacity loss and safety risks. Cyclic voltammetry (CV) and electrochemical impedance spectroscopy (EIS) are the most powerful techniques for investigating LIBs, which provide insight into redox behaviors, electrode kinetics, and internal resistance, respectively. In this study, the electrochemical performance and degradation mechanisms of a commercial 600mAh lithium-ion pouch cell were examined under controlled cycling conditions. The cell was subjected to 100 charge-discharge cycles at room temperature and 100°C, with current rates of 100mA, 300mA, and 500mA individually. The charge-discharge cycling, in particular at higher current rates and elevated temperatures, results in significant capacity fade, fluctuating Coulombic efficiency, and internal short circuits. EIS analysis showed high initial impedance due to incomplete SEI formation, and from the CV, it was concluded that the reaction kinetics and ion mobility were enhanced at higher temperatures. Severe structural degradation, such as roughening, dendritic growth, and lithium plating on the anode surface, was observed using optical microscopy, especially after high current cycling.

সারসংক্ষেপ

লি-আয়ন ব্যাটারিগুলি গ্রাহক ইলেকট্রনিক্স থেকে পুনর্নবীকরণযোগ্য শক্তি সিস্টেমের সবকিছুতে অপরিহার্য হয়ে উঠেছে। যাইহোক, তারা প্রধানত উচ্চ তাপমাত্রায় উদ্ভূত কিছু মূল কর্মক্ষমতা এবং নিরাপত্তা চ্যালেঞ্জের সম্মুখীন হয়। সাধারণভাবে, উচ্চ তাপমাত্রা গ্যাস উৎপাদন, লিথিয়াম প্লেটিং, এবং ইলেক্ট্রোলাইট ভাঙ্গনের মতো বিভিন্ন অবক্ষয় প্রক্রিয়ার গতি বৃদ্ধি করে, যার ফলে ক্ষমতা হ্রাস এবং নিরাপত্তা ঝুঁকির সৃষ্টি হয়। সাইক্লিক ভোল্টমেট্রি (সিভি) এবং ইলেক্ট্রোকেমিক্যাল ইম্পিডেন্স স্পেকট্রোস্কোপি (ইআইএস) হল এলআইবি তদন্ত করার জন্য সবচেয়ে শক্তিশালী কৌশল, যা যথাক্রমে রেডক্স আচরণ, ইলেক্ট্রোড গতিবিদ্যা এবং অভ্যন্তরীণ প্রতিরোধের অন্তর্দৃষ্টি প্রদান করে। এই গবেষণায়, একটি বাণিজ্যিক 600mAh লিথিয়াম-আয়ন পাউচ সেলের বৈদ্যুতিক রাসায়নিক কর্মক্ষমতা এবং অবক্ষয় প্রক্রিয়া নিয়ন্ত্রিত সাইক্লিং অবস্থার অধীনে পরীক্ষা করা হয়েছিল। সেলটি ঘরের তাপমাত্রা এবং 100°C এ 100টি চার্জ-ডিসচার্জ চক্রের অধীন ছিল, যার বিদ্যুৎ প্রবাহের হার 100mA, 300mA, এবং 500mA পৃথকভাবে। চার্জ-ডিসচার্জ সাইক্লিং, বিশেষ করে উচ্চ বিদ্যুৎ প্রবাহ হারে এবং উচ্চ তাপমাত্রায়, এর ফলে উল্লেখযোগ্য ক্ষমতা বিবর্ণ হয়, কুলম্বিক দক্ষতা ওঠানামা করে, এবং অভ্যন্তরীণ শর্ট সার্কিট। ইআইএস বিশ্লেষণে অসম্পূর্ণ SEI গঠনের কারণে উচ্চ প্রাথমিক প্রতিবন্ধকতা দেখা গেছে এবং সিভি থেকে এই সিদ্ধান্তে উপনীত হয়েছে যে উচ্চ তাপমাত্রায় প্রতিক্রিয়া গতি এবং আয়ন গতিশীলতা বৃদ্ধি পেয়েছে। বিশেষত উচ্চ কারেন্ট সাইক্লিং এর পরে, অপটিক্যাল মাইক্রোস্কোপি ব্যবহার করে রুক্ষতা, ডেনড্রাইটিক গ্রোথ এবং অ্যানোড পৃষ্ঠে লিথিয়াম প্লেটিং এর মতো গুরুতর কাঠামোগত অবক্ষয় লক্ষ্য করা গেছে।

Table of Contents

List of Figures

List of Tables

Chapter 1
INTRODUCTION

1.1 BACKGROUND

Demand for energy storage systems (ESS) has increased substantially over the past few years, due to unsustainable use of nonrenewable resources and the irregular availability of renewable energy sources. Fossil fuels, such as natural gas, coal, and oil, are good examples of rapidly depleting resources, and their continuous use aggravates environmental problems by polluting water supplies and emitting greenhouse gases. This has led to the necessity of a switch to clean, renewable sources of energy: solar, wind, hydroelectric, and geothermal power. However, so far, these renewable sources cannot ensure that energy supply is steady and continuous; they depend on outside factors—sometimes wind does not blow, and the sun's intensity varies throughout the day [1,2]. Energy storage systems really become a key technology in overcoming these challenges and ensuring that the supply of electricity is stable. If there is much excess energy, ESS technologies store it, and in the case of insufficient production, they release it again. This helps, through the addition of stability to the balance between supply and consumption of energy by responding quickly to any unexpected peak in demand to increase grid stability. Among other ESS technologies, tremendous interest has been shown in the ability of electrochemical energy storage, mostly batteries, to store energy and release it efficiently with low losses. The technique transforms and stores energy that can be converted back to electric form through conversion into chemical form in devices like electrochemical energy storage systems and batteries. Batteries can be broadly divided into two groups: primary batteries, which are single-use and encourage irreversible electrochemical processes, and secondary batteries, which allow for reversible reactions and repeated cycles of charging and discharging. Lithium-ion (LIB), nickel-cadmium, and nickel-metal hydride batteries are examples of secondary batteries. LIBs are now the most popular rechargeable battery option because of their increased energy density, longer cycle life, improved efficiency, and versatility for a range of uses, such as stationary energy storage systems, electric vehicles, and portable gadgets. The primary anode material for LIBs since its commercial debut by Sony in 1991 has been graphite, which is preferred due to its affordability, structural stability, and environmental friendliness. However, there are drawbacks to graphite, including as a theoretically limited capacity that limits its use in high-power devices. Moreover, volume variations could occur throughout the lithiation/delithiation process, causing stress on the electrode and diminishing cycling stability. Another

major issue is lithium plating on the graphite surface under particular circumstances, which reduces performance and raises safety hazards. By investigating new materials and creative designs, ongoing research aims to overcome these problems and enhance the LIBs' efficiency, safety, and capacity. A more sustainable energy future may be facilitated by the development of sophisticated LIB technologies, which could allow large-scale applications like the integration of renewable energy sources and next-generation electric vehicles [3–5].

1.2 ENERGY STORAGE TECHNIQUES

Devices for storing energy are made based on their capabilities and applicability. Different types of energy, including chemical, mechanical, electric, electrochemical, and thermal are shown in Fig. 1.1.

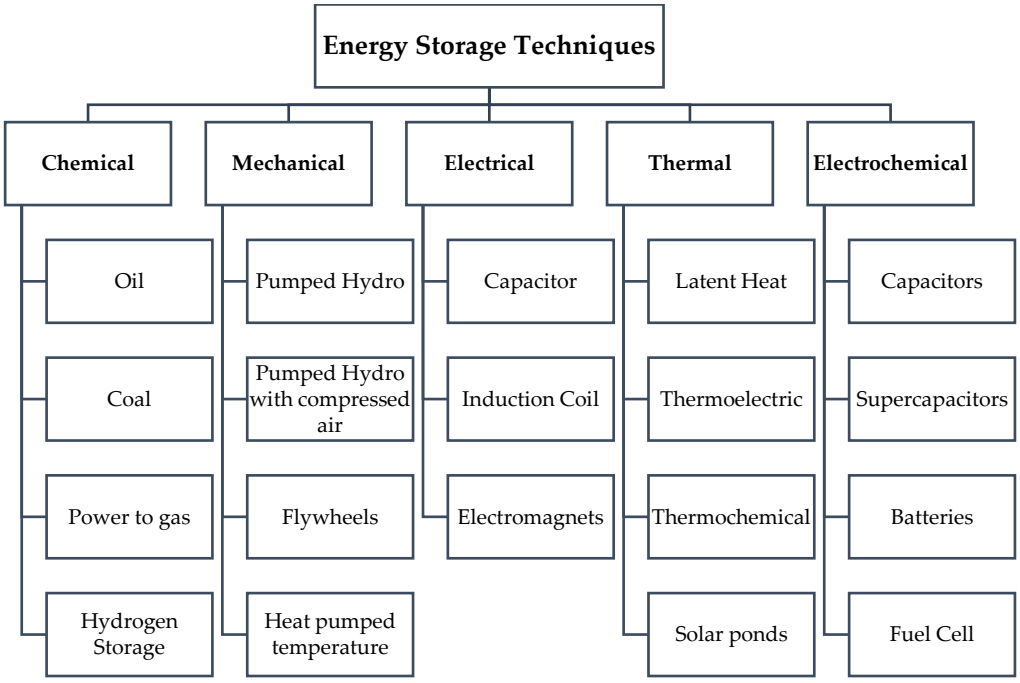

Figure 1.1 Classification of different types of energy

1.2.1 Chemical Energy

Chemical energy is dependent on the bonding between atoms or molecules and is stored in a material's structure. Energy is released during a chemical process and can be used again as heat energy or electrical energy. This energy storage process is

called thermochemical energy storage because the chemical reaction can be either endothermic or exothermic. Although it comes in a variety of fundamental forms, including coal, gas, crude oil, biomass, and others, it pollutes the environment because of its dangerous consequences [6].

1.2.2 Mechanical Energy

Kinetic energy, energy of motion, and potential energy, energy stored depending on an object's position or configuration, are the two major kinds of mechanical energy. It is the kind of energy crucial for most uses in providing transportation networks and powering machinery. Mechanical energy is useful in many systems and gadgets, from hydroelectric power plants using turbines to transform the potential energy of water stored in reservoirs into electrical power, to flywheels storing kinetic energy for later use. These mechanical energy storage devices are characterized by high-power density, reaction time, and durability, so it would be particularly interesting for applications involving fast energy discharge, like stabilization in renewable energy systems and electrical grids. Mechanical energy systems continue to evolve with each engineering and material advance, bringing effective and sustainable solutions to the energy conundrums facing us today [6].

1.2.3 Electric Energy

All modern appliances and industrial systems in the world are driven by electric energy, generated from the movement of electric charges. It is an efficient way to distribute it through power networks and to be produced by nuclear, fossil fuels, and renewable energy sources. Because it can be easily transformed into chemical, thermal, or mechanical energy, it becomes very versatile. Technological innovation on storage technologies—batteries, in particular—make them functional, fostering sustainability and integration with renewable energy [6].

1.2.4 Thermal Energy

The energy associated with the motion of particles in a substance is commonly called thermal energy or heat energy. It is the primal source of energy; hence, it may also be used for different purposes, such as in processes by industries, generation of power, and heating. Fossil fuel burning, geothermal reservoirs, and solar thermal systems would be some good examples. Energy can be used when needed because it can be stored in such substances as water or molten salts. Thermal energy plays a vital role

and has been a significant component in modern-day energy solutions, mainly in systems such as power plants and heating networks [7].

1.2.5 Electrochemical Energy

Most of the modern energy systems depend on the electrochemical energy storage devices in which chemical energy is converted to electrical energy via electrochemical reactions. Due to their high energy density, scalability, fast charge–discharge cycles, and environmental advantages, technologies such as fuel cells, capacitors, supercapacitors, and batteries have revolutionized the way in which energy is stored and delivered. Two terms that define ESSs are depicted bilaterally in Fig.1.2, comparing a number of ESSs. The first is specific power, also called power density, which expresses how much power a system can deliver per unit of weight. Second comes the specific energy, which describes how much energy the system can store internally. It is not necessary to have a high value of energy, but the higher the energy density of the systems, the longer they will be able to provide energy. Also, more power can be drawn from the system as the power density is higher, and vice versa. In the event that the goal is to store energy for a longer time, ESSs with high specific energy may be the best choice. [3–5].

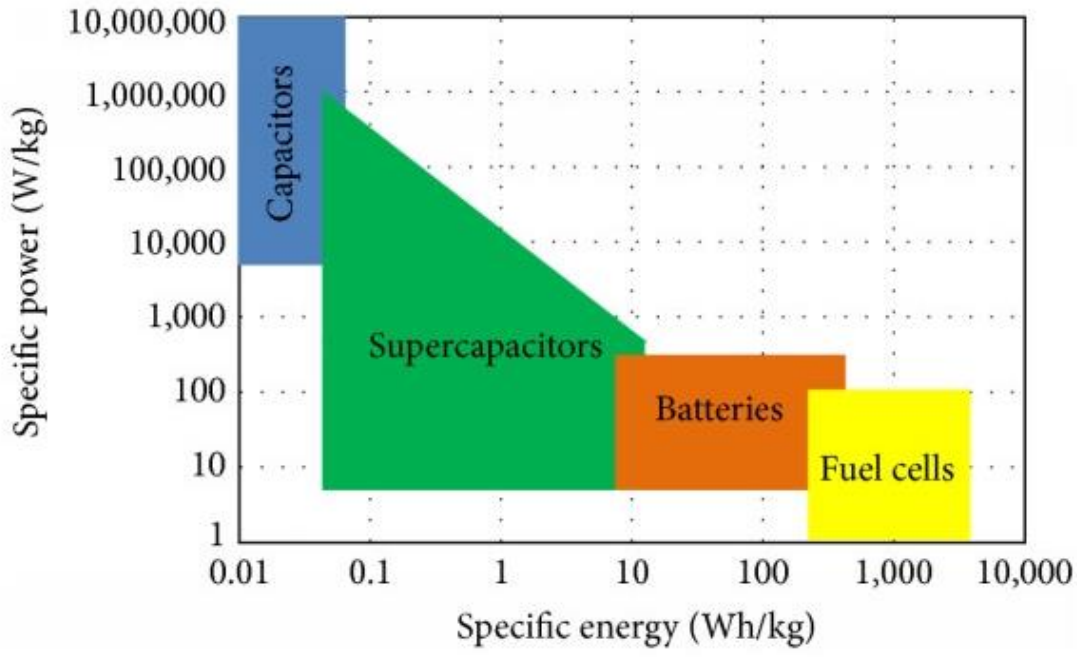

Figure 1.2 Energy storage and conversion devices with specific energy and power [8]

1.2.5.1 Capacitors

Capacitors store energy electrostatically by building up charge on conductive plates separated by a dielectric material and are thus indispensable to most modern electronic systems. Due to their quick charge-discharge capability, they play a very important role in the regulation of voltage, smoothing of power, and delivering transient energy. But, because of their low energy density, they can be used only for very short-term energy purposes [9,10].

1.2.5.2 Supercapacitors

Supercapacitors possess much higher energy density compared to conventional capacitors and batteries, yet retain the fast charge-discharge capability of the latter. They store energy through electrostatic and electrochemical means using high-surface-area electrodes and an electrolyte. Their long cycle life and robustness make them very suitable for applications such as grid stability, regenerative braking, and high-power electronics [11,12].

1.2.5.3 Fuel Cell

Fuel cells represent a promising solution for electrochemical devices that can generate electricity continuously from the reaction of fuel-fuel usually hydrogen-with an oxidant, normally oxygen, for clean energy applications in transportation, stationary power generation, and industrial processes, since they do not internally store energy but obtain it from an external fuel supply, which permits operation for as long as it is fed [13].

1.2.5.4 Battery

Moving from fossil fuels to renewable energy requires an efficient energy system, with modern battery storage technology. In view of the ever-growing demands for power and creation of renewable energy, the importance of battery storage will keep on growing. The energy storage device may be used either as a unit to store energy from a generator or as the energy source in a system. For example, energy storage in a lithium-ion battery can be used to run a cell phone while another one in a lead-acid battery can supply the needs for a car. Among the advantages of energy storage over fuel is that it is more renewable since it recharges without requiring more material inputs into its system. Figure 1.3 shows the batteries' energy densities for a comparative visual representation.

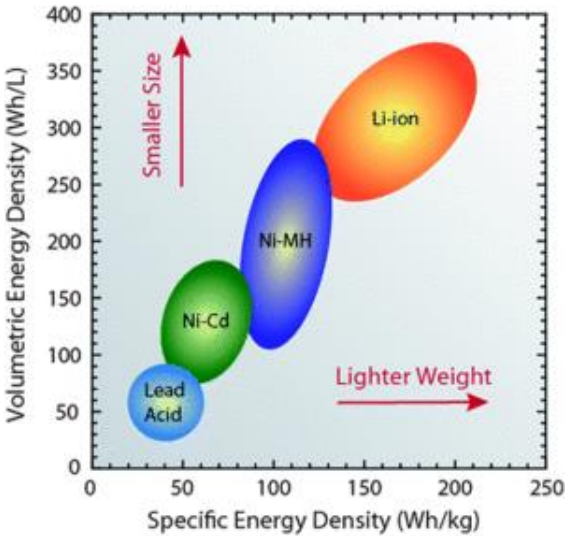

Figure 1.3 Comparison of four popular battery types' energy densities [14]

1.2.5.4.1 Lead Acid Battery

The lead-acid battery is among the oldest and most common types of rechargeable batteries. They contain lead dioxide, PbO_2, as the positive electrode, sponge lead, Pb, as the negative electrode, and an electrolyte solution prepared from sulfuric acid, H_2SO_4. Because they have very high surge currents, these batteries are used for applications that require large bursts of energy, such as automobile, truck, and motorcycle starters. Another purpose for which lead-acid batteries are widely used includes uninterruptible power systems, backup power supplies, and renewable energy storage systems. For all their cheapness and reliability, the energy density of lead-acid batteries is extremely low-a lot less energy stored in their size when compared to more modern technologies such as lithium-ion batteries. They are also vulnerable to sulfation, which can reduce their lifespan by resulting in the formation of lead sulfate crystals on the electrodes. Furthermore, lead is toxic, and improper disposal of lead-acid batteries can contaminate the environment. Despite these drawbacks, many applications continue to favor lead-acid batteries due to their affordability, tested technology, and recyclability [15,16].

1.2.5.4.2 Ni-Cd Battery

One variety of secondary battery is the nickel-cadmium or Ni-Cd battery, in which the negative electrode is made of cadmium and the positive electrode is nickel oxide hydroxide. Due to its resistance to degradation with repeated charge/discharge cycles and its reputation for ruggedness, Ni-Cd batteries are applied in many uses similar to power tools, emergency lighting, and aviation systems. They operate well over a wide range of temperatures and can withstand severe conditions. However,

Ni-Cd batteries are prone to the so-called "memory effect," wherein a partial discharge over time gradually reduces their usable capacity. Besides that, cadmium is a toxic heavy metal that poses environmental concerns with regard to its recycling and disposal, uses that have been on the decline in favor of greener alternatives such as lithium-ion batteries. Despite these disadvantages, for industrial and aerospace purposes requiring reliability and high efficiency, the Ni-Cd batteries have remained an unmatched means of energy storage to date [17,18].

1.2.5.4.3 Ni-MH Battery

Nickel-metal hydride batteries are a type of rechargeable battery, wherein their negative electrode is made from a hydrogen-absorbing alloy, while the positive electrode is nickel oxide hydroxide. Compared with nickel-cadmium, or Ni-Cd batteries, these batteries have higher energy density, which makes them the popular option for consumer electronics, hybrid cars, and even rechargeable power tools. Because they don't contain cadmium, the hazardous materials in Ni-Cd, Ni-MH batteries prove to be more environmentally friendly. Their reduced memory effect enables them to handle more flexible cycles of charging and discharging. However, their energy density is lower compared to lithium-ion batteries, and their functionality may be affected by changes in temperature. Due to their affordable cost, reliable performance, and safety features, Ni-MH batteries remain in wide use for a variety of consumer and commercial applications [19,20].

1.2.5.4.4 Lithium Ion Battery

Li-ion batteries have wide applications in consumer electronics, EVs, and energy storage systems in recent time due to their light weight and high energy density, with long cycle life. These batteries use graphite as negative electrode (anode), lithium compounds-such as lithium cobalt oxide or lithium iron phosphate-as positive electrode (cathode), and organic solvent-based lithium salt as the electrolyte. Electrical energy is generated when lithium ions flow through the electrolyte from the anode to the cathode during a discharge and in the opposite direction during charging. Compared to older battery technologies like nickel-cadmium and lead-acid batteries, Li-ion batteries boast several advantages: superior energy density, longer life, and no memory effect. Because of that, they can store more energy in relation to one unit of weight and volume; for that, they will suit grid energy storage perfectly well, electric vehicles, and portable electronics. The fact that overcharge and too high a temperature might badly influence its quality-performing, they easily give into explosions like thermal runaway. The continuous leading place of Li-ion batteries

among other technologies is due to their effectiveness, scalability, and wide utilization in diverse industries despite such obstacles [21–23].

1.3 WORKING PRINCIPLE OF LIB

Lithium, a silvery, white alkali soft metal, is the lightest metal and solid under some standard conditions. According to the electrochemical series, it has the highest tendency to lose electrons. It is highly reactive in its pure form but quite stable when it is a part of metal oxide [24]. Because of these special qualities, lithium is crucial for creating advanced devices for storing energy, especially lithium-ion batteries. Lithium compound-based cathodes such as lithium cobalt oxide (LCO), carbon-based anodes such as graphite, electrolyte, and separator are the basic component of a lithium-ion battery. Aluminum and copper foil act as a current collector, where cathode and anode material are coated, respectively. Fig. 1.4 illustrates the charging and discharging mechanism of a lithium-ion battery. During the charging and discharging cycles, lithium ions are successively intercalated and deintercalated. During charging, electrons move from cathode to anode by the external circuit. Then the Li^+ is free from the metal oxide which is usually used as a cathode. After that, it goes through the electrolyte and the separator to the anode where it will be stored. The separator is semi-permeable because only Li^+ can pass through it, but e^- cannot. Since the separator does not allow Li^+ and e^- to be connected, as a result, the internal short circuit is prevented. The reverse process occurs during discharging [25].

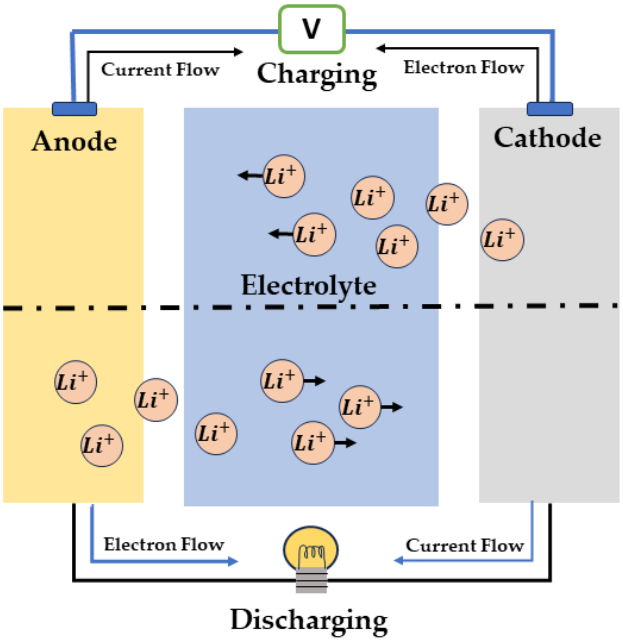

Figure 1.4 LIBs operating mechanism

Redox reactions occur during the charging and discharging of LIBs at the electrode which is showed between Eqn. (1-4) [26], examples given for Lithium Iron Phosphate (LFP) battery.

Charging:

$$\mathrm{Li_yFePO_4} \rightarrow Li_{y-z}FePO_4 + zLi^+ + ze^- \quad (1)$$

$$\mathrm{Li_{x-z}C_6 + zLi^+ + ze^-} \rightarrow \mathrm{Li_xC_6} \quad (2)$$

Discharging:

$$\mathrm{Li_yFePO_4} \leftarrow Li_{y-z}FePO_4 + zLi^+ + ze^- \quad (3)$$

$$\mathrm{Li_{x-z}C_6 + zLi^+ + ze^-} \leftarrow \mathrm{Li_xC_6} \quad (4)$$

1.4 LI-ION BATTERIES OF DIFFERENT SHAPES

Li-ion batteries are available on the market in a variety of sizes and shapes. These are the coin cell, pouch cell, prismatic cell, and cylindrical cell, as seen in figure 1.5. Common forms of cylindrical cells include A, AA, AAA, AAAA, B, C, 18650, and so on. As seen in figure 1.5 (a), a pouch Li-ion battery cell with 600mAh capacity was selected for this investigation.

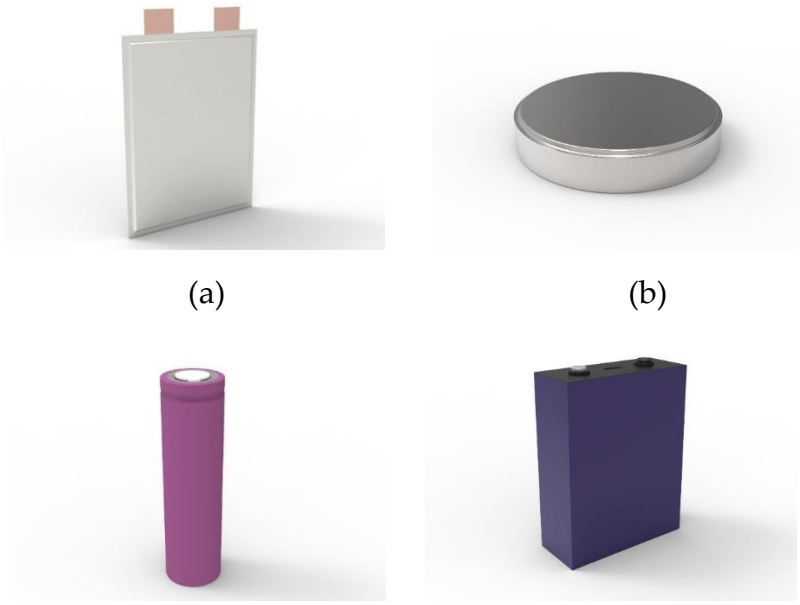

(a) (b)

(c) (d)

Figure 1.5 (a) Pouch Cell (b) Coin Cell (c) 18650 Cylindrical Cell (d) Prismatic Cell

1.5 MOTIVATION AND OBJECTIVES

LIBs have performance and safety issues, particularly in high temperature conditions. Elevated temperatures increase the processes of degradation, including as gas production, lithium plating, and electrolyte breakdown, which eventually lowers battery capacity and raises safety concerns. Cyclic Voltammetry (CV) and Electrochemical Impedance Spectroscopy (EIS) are effective methods for examining the internal dynamics of LIBs. CV shows redox behaviors and electrode kinetics, whereas EIS sheds light on internal resistance, diffusion processes, and charge transfer resistance. Nevertheless, the combined application of these methods at high temperatures is still little studied for the commercially available batteries, which presents a chance to improve our knowledge of LIB behavior and degradation processes. Research objectives of this study include the following terms:

- To investigate the effects of elevated temperatures on the electrochemical behavior of commercial LIBs using EIS and CV techniques.
- To analyze changes in internal resistance, charge transfer kinetics, and degradation mechanisms at different temperature conditions.

1.6 THESIS OUTLINE

This thesis, titled "Study of Electrochemical Impedance Spectroscopy and Cyclic Voltammetry of Commercial Lithium-ion Battery at Elevated Temperature," explores the principles and applications of EIS and CV to investigate the electrochemical performance of lithium-ion batteries. The thesis is organized as follows:

Chapter-01: Introduction

This chapter introduces various types of electric energy storage systems, highlighting their advantages and limitations. It emphasizes the importance of energy storage in facilitating renewable energy integration and discusses lithium-ion batteries as a promising technology for energy storage applications.

Chapter-02: Literature Review

This chapter provides an overview of internal resistance measurement techniques for lithium-ion batteries, with a focus on Electrochemical Impedance Spectroscopy (EIS) and Cyclic Voltammetry (CV). Relevant studies and advancements in the field are reviewed.

Chapter 3: Methodology

This chapter outlines the experimental procedures, including details of the experimental setups, data collection methods, and the equipment used during the study.

Chapter 4: Results and Discussions

This chapter provides a detailed interpretation of the experimental results, discussing their implications and comparing them with findings from previous studies.

Chapter 5: Conclusion and Future Study

This chapter summarizes the key findings of the research, discusses its limitations, and provides recommendations for future studies to build on the current work.

Chapter 2

Literature Review

2.1 INTRODUCTION

The measurement of internal resistance and thermal effects being the emphases of this chapter, it now seeks to comprehensively analyze the body of research on lithium-ion batteries. The chapter opens with a look at how temperature influences LIB performance, safety, and degradation mechanisms to demonstrate the vital necessity for temperature control in battery systems. It then proceeds to discuss some of the methods of determining internal resistance, outlining their principles, advantages, and shortcomings. The basic concepts, measurement techniques, and interpretation of impedance spectra of EIS and CV are discussed in detail herein. This section shall help to elucidate the flexibility and accuracy of EIS as a diagnostic tool for LIBs. It also looks into how EIS and CV are being applied in battery research and industry, pointing out how it is used in performance assessment, degradation analysis, and in the development of new pioneering battery technologies.

2.2 EFFECT OF TEMPERATURE ON LIBS

Complex electrochemical changes take place during the charging and discharging of a LIB with a significant quantity of heat release. The performance, longevity, as well as safety of a Lithium-ion battery, is affected by the operating or ambient temperature [26]. Temperature also affects the ionic conductivities of electrodes and electrolytes [27]. In Fig. 2.1, some temperature effects are illustrated which will be discussed in the following sections.

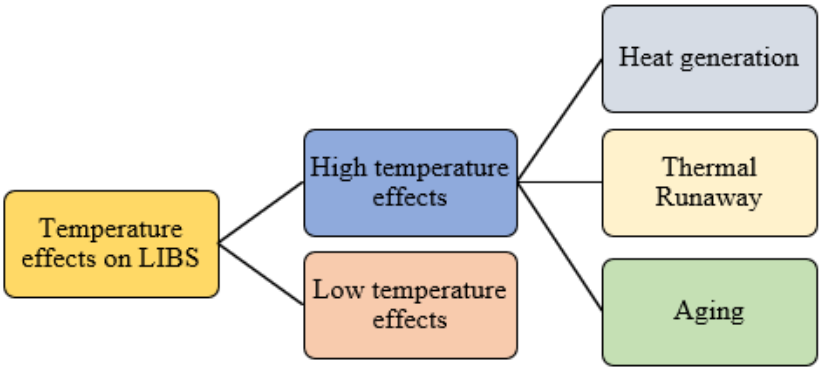

Figure 2.1 Effects of temperature on LIBs.

2.2.1 *Effects of Low Temperature*

The properties of electrolytes are affected when the battery is exposed to cold temperatures. At low temperatures, the internal resistance of the electrolyte rises due to its viscosity. As a result, the Lithium-ion diffusivity and the electrolyte's ionic conductivity, power, and capacity of the cell decreases [28–30]. The charge transfer resistance (R_{ct}) is one of the most significant factors that also increase at low temperatures [31]. Zhang et al. [31] interpreted by their experiment that, it is more difficult to charge a drained Li-ion battery than it is to discharge a charged battery at a low temperature. Petzl et al. [32] demonstrated that at low temperatures, lithium plating occurs. Lithium plating has the ability to penetrate separators and reduce capacity. These lithium dendrites, which are located on the surface of the negative electrode of LIBs, cause an internal short circuit [33].

2.2.2 *Effects of High Temperature*

High temperatures impair the performance of Lithium-ion batteries more than low temperatures. So, it's crucial to research LIBs behavior at high temperatures. In this section, some high-temperature effects are discussed.

2.2.2.1 Heat Generation

At room or standard operating temperature, electrochemical reactions and charge transfer produce heat inside the battery [34]. Irreversible processes like heating due to mixing, polarization, enthalpy change, etc. are also responsible for generating heat. In fig. 2.2 some causes for generating heat are illustrated. Xiao and Choe [34] were proposed a completely new heat generation formulation, which incorporates enthalpy heating and heat of mixing.

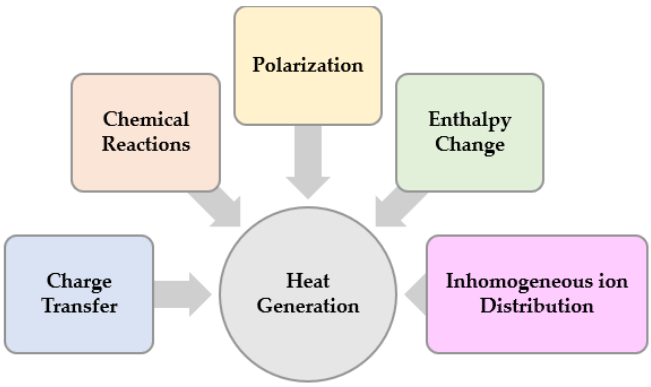

Figure 2.2 Various heat generation process

2.2.2.2 Thermal Runaway

Thermal runway is another destructive phenomenon for a lithium-ion battery. It occurs when the heat formed inside a battery surpasses the quantity of heat released to its surroundings [35]. In Fig. 2.3 thermal runaway process of a LIBs cell is illustrated. At high temperatures, exothermic reactions occur in the battery and uncontrollable heat is produced. Also, internal pressure is increased due to the production of some gaseous elements. As a result, exploration would occur [36]. Feng et al. [37] observed that during thermal runaway the internal temperature was gone above 870˚C and the difference of temperature was 520˚C inside the tested battery.

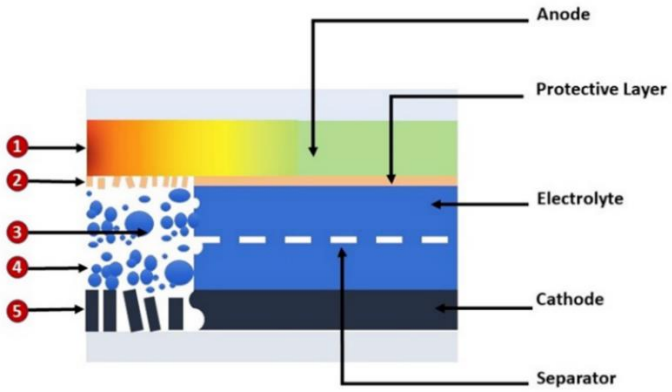

Figure 2.3 The thermal runaway process of lithium-ion batteries (numbers here indicate: 1. Heating starts; 2. The protective layer dissolves; 3. Flammable gas is created when electrolytes split; 4. Separator melts could cause short circuits; and 5. The cathode breaks down and releases oxygen [38] .

Figure 2.4 depicts that when a cell failure due to thermal runaway and if it propagates to the other cell of the battery, it may destroy the whole battery.

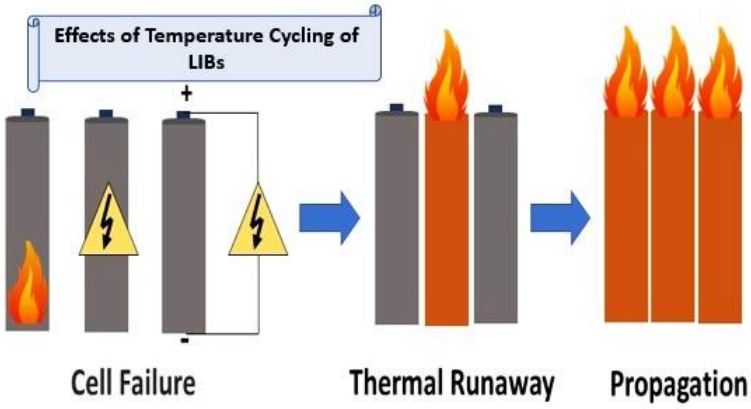

Figure 2.4 Destruction of a battery due to thermal runaway [38].

At high temperatures, LIBs lifespan, as well as performance, are reduced due to aging. Leng et al. [39] found by their investigation that, when a Sony Prismatic lithium-ion battery was aged from 25˚C to 55˚C, it's capacity degraded due to the temperature impact. Bondenes et al. [40] found by their experiment that the battery capacity was lost by around 7.5% at 85°C. But when cycled at 120˚C the loss of capacity reached 22%. They used Li (Ni, Mn, Co) O_2 (NMC) based lithium-ion batteries for the analysis of the aging process.

2.3 METHODS FOR MEASURING THE INTERNAL TEMPERATURE OF LIBS

Measuring techniques of a battery's internal temperature is complicated compared to the surface temperature due to its multilayered structures. Using thermocouples and thermal imaging systems, the surface temperature of LIBs can be easily measured [41]. Various methods for measuring a battery's interior temperature are demonstrated in Fig. 2.5.

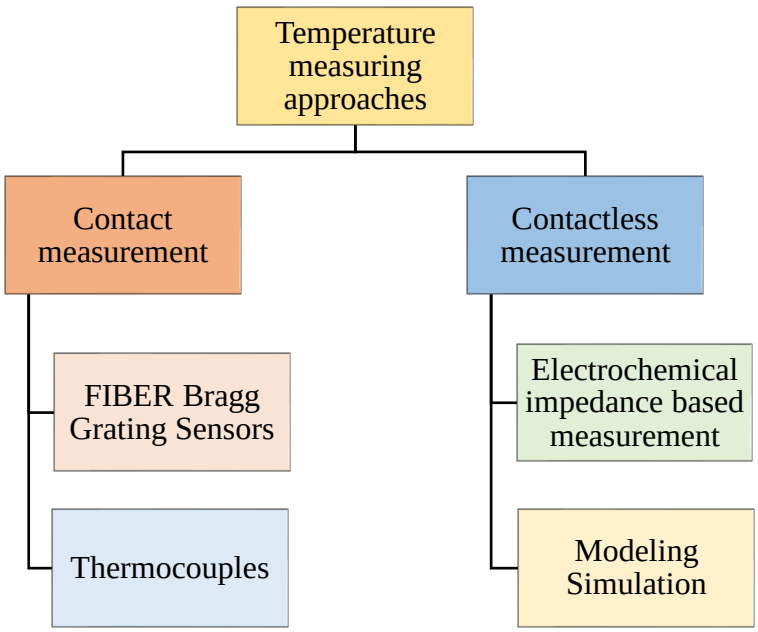

Figure 2.5 Current methods for monitoring the interior temperature of LIBs.

To detect the temperature by contact measurement, temperature sensors such as Fiber Bragg Grating (FBG) sensors or thermocouples are placed within LIBs. But, the structural integrity of LIBs can be damaged by the insertion of heat sensors [42]. That's why electrochemical impedance-based and modeling simulation techniques are developed to eliminate the damage to the internal structure of the LIBs.

The thermal model and the thermal-electric model are the two numerical models that are developed by the researchers for determining the internal temperature of LIBs. In the thermal model, only thermal and in the thermal-electric model thermal as well as electric characteristics inside batteries can be predicted [43,44].

2.4 METHODS FOR MEASURING THE INTERNAL RESISTANCE OF LIBS

Internal resistance is one of the most determining factors for power, energy efficiency, and lost heat of the lithium-ion cell. It can be measured for the cell by means of the current step method, alternating current method (AC), heat loss method and electrochemical impedance spectroscopy (EIS) method.

2.4.1 Current Step Method

One of the most straightforward and widely applied methods to measure internal resistance at present is the step current method. In this approach, a step current-that is, a sudden alteration of current-is applied to the battery, and then the voltage response to it is monitored. By Ohm's law (eqn. 5), internal resistance R can be computed as,

$$R = \frac{\Delta V}{\Delta I} \tag{5}$$

Where,

ΔV is change in voltage

ΔI is change in current.

In practice, a step current is applied, and the voltage drop across the battery is measured immediately after applying the current. This gives an estimation of the internal resistance by how the voltage of the battery responds to a sudden change in current. This technique is very effective for rapid, rough estimates of internal resistance but is less valid under conditions of large changes in either state of charge or temperature [45,46].

2.4.2 AC Method

The AC method, on the other hand, is where the internal resistance of the battery is obtained using a very small, alternating current signal. This means that when the sinusoidal current frequency has been applied onto the battery, it measures voltage response. It will be learned on AC excitation how voltage-to-current can provide information related to battery impedance, comprising internal resistance and other electrochemical phenomena [47].

At a specific frequency, the impedance Z(ω) can be expressed as (eqn. 6),

$$Z(\omega) = R + jX(\omega) \tag{6}$$

Where,

R is the internal resistance

$X(\omega)$ is the reactance, which depends on the frequency

j is the imaginary unit

The internal resistance can be determined either by analyzing the phase shift between the applied current and the voltage response or, alternatively, by looking at the amplitude of the voltage. This approach is a very important one, as it gives information regarding the resistance and the capacitive and inductive behaviors of a battery over a range of frequencies. It is designed to identify the resistive losses as well as the dynamic behavior, including charge transfer and diffusion effects, that will affect the performance of a battery under different operating conditions [47].

2.4.3 Thermal Loss Method

The thermal-loss method calculates the internal resistance of a battery by observing the heat produced while the battery charges and discharges. This is because internal resistance causes energy losses in the form of heat—known as Joule heating. The amount of heat can thus be correlated with the internal resistance [48].

The basic principle is that whenever a current flows across a resistive material, it generates heat according to Joule's law (eqn. 7)

$$Q = I^2Rt \tag{7}$$

Where,

Q is the heat generated

I is the current

R is the internal resistance

t is the time for which the current flows

Heat generation in lithium-ion batteries originates from both Joule's heating and chemical reactions; the latter can be exothermic or endothermic. During charging, the reversible heat effect starts as endothermic and becomes slightly exothermic, reversing during discharge. Under high current loads, Joule's heating dominates, making it the primary focus for internal resistance measurements using calorimetry [49–51]. A calorimeter shown in figure 2.6, consisting of a Dewar vessel, stirrer, and thermometer, measures heat generated by the battery based on temperature changes and known heat capacities. Calibration ensures accuracy, and alternating current is used for heat dissipation in long-term measurements to determine internal resistance accurately [52].

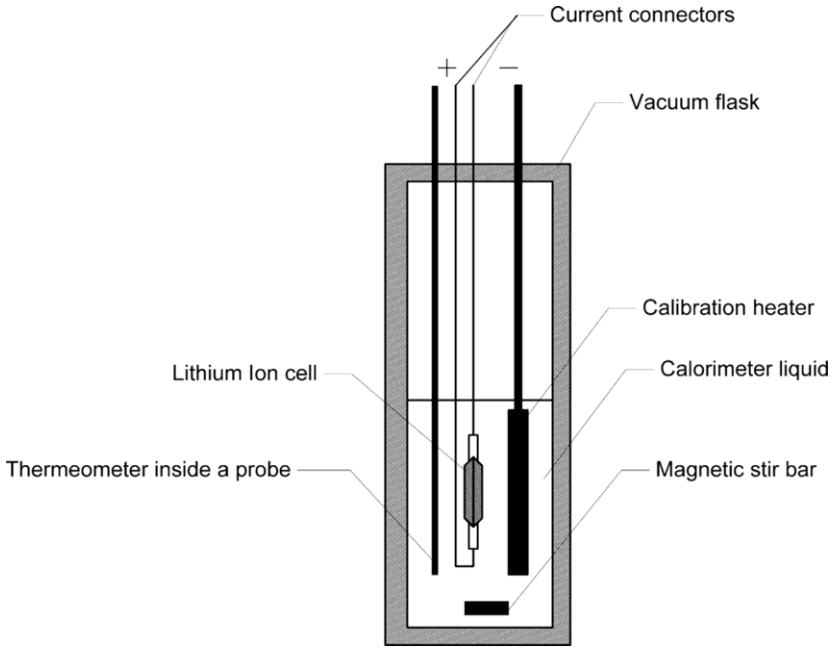

Figure 2.6 Quasi-adiabatic calorimetry for measuring heat generation in batteries [46]

The calorimeter's heat capacity is represented by C_{cal}. Using a lithium-ion cell whose heat capacities have been measured by prior tests and calorimeter measurements with a substance called calorimeter liquid, one must calculate the temperature change during the cell's charge/discharge cycle in order to calculate the value of R_i from the known values of C_{cell}, C_{cal}, ΔT, and Q. Because of the limited energy capacity of the cell under test, Equation (7) and the derived Equation (8) for calorimeter testing with constant current are unsuitable for long-term measurements. Consequently, alternating current was employed to generate heat dissipation, as described in Equation (9).

$$Q = I^2Rt = (C_{cal} + C_{cell}) \times \Delta T \tag{8}$$

$$Q_{loss} = \int_{t_1}^{t_2} (I\ (t)^2 . R_t . dt) = (C_{cal} + C_{cell}) \times (T_2 - T_1) \tag{9}$$

The cell's internal resistance can be computed by converting Equation (9):

$$R_t = \frac{(C_{cal} + C_{cell}) \times (T_2 - T_1)}{\int_{t_1}^{t_2} I\ (t)^2 . dt} \tag{10}$$

2.4.4 Electrochemical Impedance Spectroscopy Method

Electrochemical Impedance Spectroscopy (EIS) is among the most precise and popular methods of internal resistance measurement for lithium-ion batteries, which gives detailed insight into the electrochemical processes taking place inside the battery. EIS applies a small sinusoidal voltage (or current) perturbation across a wide range of frequencies and measures the corresponding current (or voltage). The impedance is calculated by analyzing the frequency response.

2.4.4.1 Principle of EIS

A key component of lithium-ion batteries that affects their kinetic performance, stability, energy density, and capacity for storing charge is double layer capacitance, which plays an important role in determining the overall performance of LIBs. Double layer capacitance develops at the contact of an electrode and an electrolyte as

shown in Fig. 2.7. Ions from the electrolyte build up at the electrode surface in response to an applied voltage, creating a double layer. This layer is composed of two areas: the outer Helmholtz plane (OHP), where solvated ions are drawn to the electrode's electric field but do not come into direct contact with the surface, and the inner Helmholtz plane (IHP), where ions are selectively adsorbed onto the electrode surface. This double layer's capacitance is similar to that of a parallel plate capacitor, in which the separation distance is the total of the ion and solvation shell effective radii, and the electrode and accumulated ions serve as the plates [53,54].

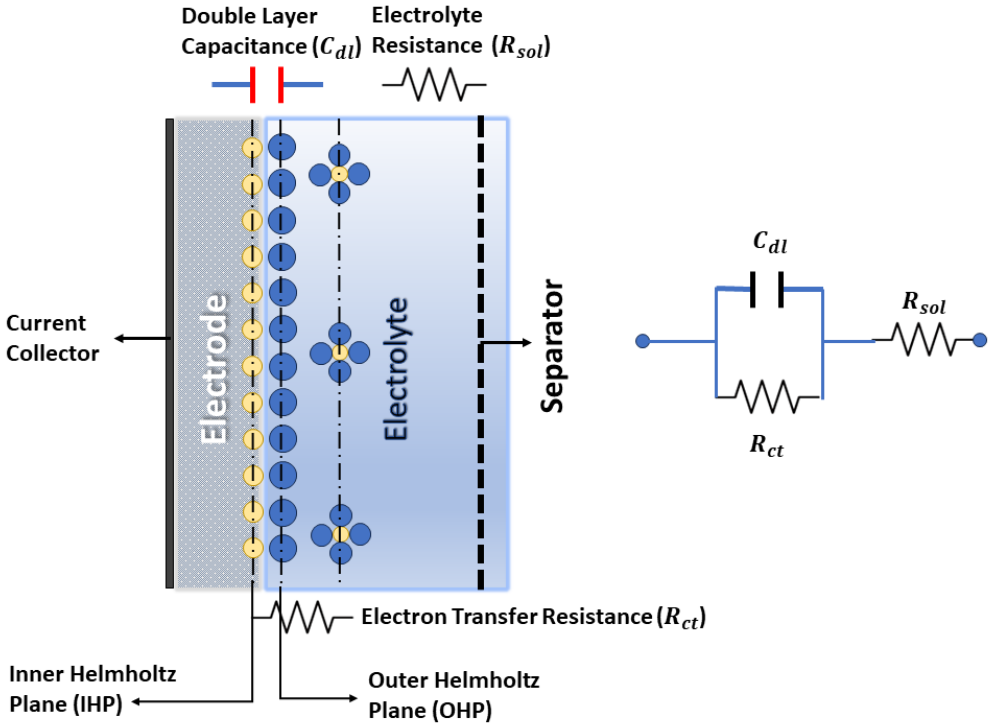

Figure 2.7 Double layer Capacitance (Adapted from [55])

In a conventional electrochemical cell, interactions between redox species and the electrode, including concentration, charge transfer, mass transfer, and electrolyte resistance, are modeled using an equivalent circuit of resistances, capacitors, and constant phase elements. Therefore, mass-transfer, charge-transfer, and diffusion processes can all be investigated using Electrochemical Impedance Spectroscopy, which can analyze inherent material characteristics or specific mechanisms affecting an electrochemical system's conductance, resistance, or capacitance.

The standard method for measuring electrochemical impedance involves subjecting an electrochemical cell to an AC voltage and then monitoring the current flowing through the cell. A little excitation signal is typically used to assess electrochemical

impedance. This is done to provide a pseudo-linear response from the cell. A sinusoid with the same frequency but a phase shift will be the current response to a sinusoidal potential in a pseudo-linear system.

DC circuits are less complex, featuring pure resistance, constant voltage and current. In contrast, alternating current and voltage, impedance made up of reactance and resistance, and frequency-dependent behavior are all present in AC circuits. Ohm's Law is used to compare DC and AC circuits, and the results show major differences in their analysis and behavior which is presented in Table 2.1.

Table 2.1 Difference between DC and AC signal

Parameter	**Direct Current (DC)**	**Alternating Current (AC)**
Current Flow	Unidirectional	Bidirectional
Voltage	Constant	Changes sinusoidally with time
Resistance/ Impedance	Pure resistance (R)	Impedance (Z) includes Resistance (R), Inductance (L), and Capacitance (C)
Ohm's Law	$R = \frac{V}{I}$	$Z(\omega) = \frac{V(\omega)}{I(\omega)} = \frac{V_0 \sin(\omega t)}{I_0 \sin(\omega t)}$ Where, $\omega = 2\pi f$
Schematic Diagram	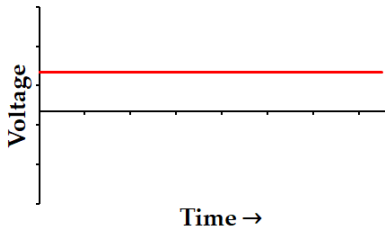	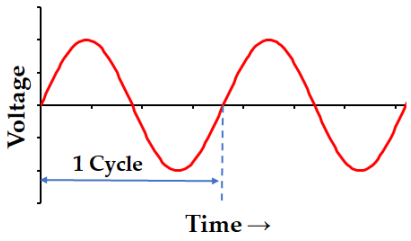

Since AC ensures linear responses, captures phase relationships, distinguishes between different impedance components, and provides frequency-dependent impedance measurements, it is employed in electrochemical systems analysis (EIS), where the excitation signal as a function of time is like equation 11.

$$V_t = V_0 \sin(\omega t) \tag{11}$$

The signal in a linear system has an amplitude that differs from I_0 and is phase-shifted (ϕ) shown in equation 12.

$$I_t = I_0 \sin(\omega t + \phi) \tag{12}$$

Figure 2.8 illustrates the phase shift in the output signal caused by the internal resistance of the battery.

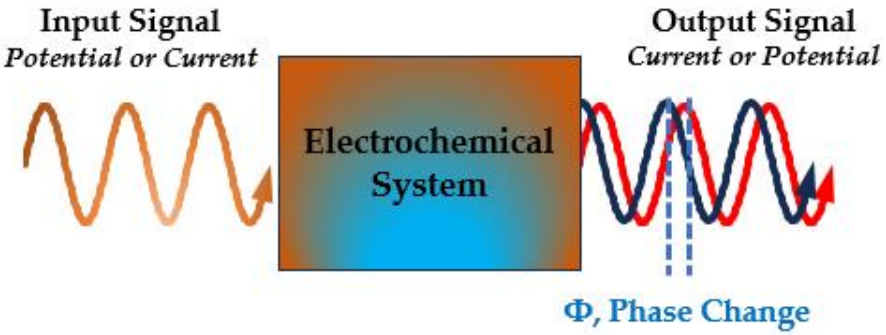

Figure 2.8 Simplified diagram of EIS where the phase angle is marked to indicate the delay between the input and output signal.

V and I for the AC circuit model in equation 11 and 12 satisfy Ohm's law. Consequently, the impedance Z(ω) can be written as follows:

$$Z(\omega) = \frac{V_0 \sin(\omega t)}{I_0 \sin(\omega t + \phi)} = Z_0 \frac{\sin(\omega t)}{\sin(\omega t + \phi)} \tag{13}$$

According to Euler's formula,

$$e^{j\phi} = \cos(\phi) + j \sin(\phi) \tag{14}$$

Where, $j = \sqrt{-1} = e^{\frac{j\pi}{2}}$

The impedance Z(ω) from equation 13 can be represented as a complex function

$$Z(\omega) = Z_0 \frac{e^{j\omega t}}{e^{j(\omega t+\phi)}} = Z_0\, e^{j\phi} \tag{15}$$

$$= Z_0 \cos(\phi) + j\ Z_0 \sin(\phi)$$

Where, $Z_0 \cos(\phi)$ is the real part (Z_{Real}) that represents the resistance, and $Z_0 \sin(\phi)$ is the imaginary part (Z_{Im}) that represents the combined effects of inductance and capacitance. An X-axis plot of the real part (Z_{Real}) and a Y-axis plot of the imaginary part (Z_{Im}) results in a Nyquist Plot depicted in figure 2.9(a). On the Nyquist plot, every point represents an impedance value at a given frequency, whereas the Z_{Im} is negative. Impedance is conducted at low frequency on the right side of the plot along the X-axis, while its generated impedances are exerted on the left at higher frequencies. Furthermore, impedance on a Nyquist plot can be depicted as an arrow with a length of |Z|, where the angle formed between this arrow and the X-axis is referred to as the phase angle.

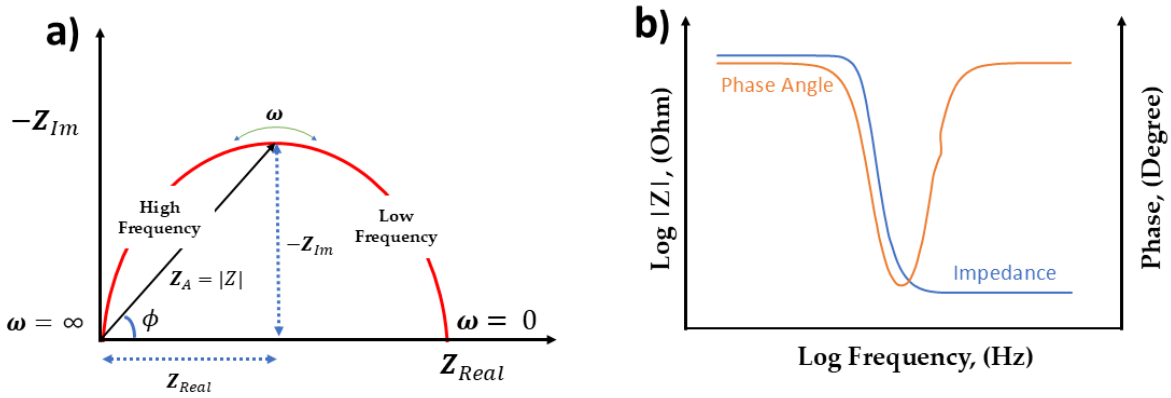

Figure 2.9 a) Nyquist Plot, and b) Bode Plot (Adapted from [56])

An alternative method of expressing the impedance data is the Bode plot, which is more popular in the engineering community than the Nyquist plot. The Bode plot consists of two distinct logarithmic plots: phase vs. frequency and magnitude vs. frequency shown in Figure 2.9(b).

2.4.4.2 EIS Application to LIBs

An effective method for examining the electrochemical characteristics and processes of lithium-ion batteries is electrochemical impedance spectroscopy, or EIS. By measuring the battery's impedance as a function of frequency, it provides insight into the internal mechanisms that control battery performance and degradation.

2.4.4.2.1 SEI Layer Formation

Lithium-ion batteries (LIBs) experience considerable performance loss during the span of their lifetime application due to unwanted chemical interactions, aging, corrosion, compromised structural integrity, and the possibility of thermal runaway. Performance deteriorates as a result of the creation of a new SEI layer, which grows and increases the internal resistance and capacity loss of LIBs. The electrochemical impedance spectroscopy technique can be used to study the formation of the solid electrolyte interface (SEI) on the electrode surface. The R_{SEI} is represented by the high-frequency intercept on the real axis shown in Figure 2.10, which is frequently the endpoint of the semicircle [57–59].

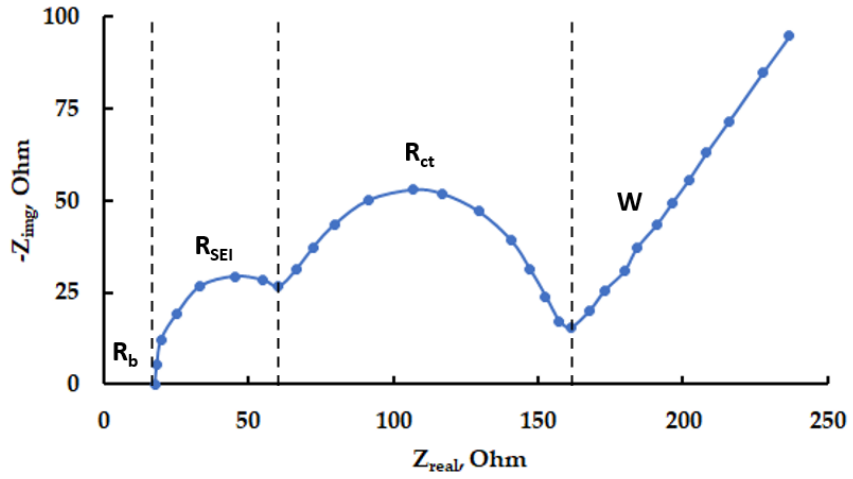

Figure 2.10 Nyquist plot of a LIBs half-cell system (Adapted from [56])

2.4.4.2.2 Cell resistance of the bulk (R_b), Charge transfer reaction (R_{ct}), and Diffusion process (W)

With EIS, every internal resistance component can be recognized and examined using unique frequency-dependent patterns in the Nyquist plot. Three main components make up the internal resistance of LIBs: the charge transfer resistance, which controls the electrochemical reaction at the electrode-electrolyte interface; the Warburg impedance (*W*), which is related to the diffusion of lithium ions within the electrode material; and the bulk resistance of the cell, which is impacted by the electrolyte and other conductive materials [53,60].

Ohmic resistance, or bulk resistance, R_b, defines the resistance of the cell's electrolyte, separator, and current collectors. The electrolyte composition, temperature, and state of health (SoH) of the battery can all influence this value. In an EIS measurement, R_b represents the aggregate of the electrolyte and additional ohmic resistances within the cell, as seen by the high-frequency intercept on the real axis of the Nyquist plot. It

is commonly observed in the impedance spectra at the highest frequency range depicted in Figure 2.10 [61].

At the electrode-electrolyte interface, where lithium ions cross the boundary, an electrochemical process takes place that is related to the charge transfer resistance, or R_{ct}. Temperature, electrolyte properties, and electrode material can all have a significant impact on this resistance, which is crucial for figuring out the reaction kinetics. R_{ct} typically appears in the medium to low-frequency range and appears as a section of a semicircle in the Nyquist plot illustrated in figure 2.10. By providing information on the electrode's ability to promote lithium-ion exchange, the diameter of this semicircle immediately reveals the value of R_{ct} [62].

The Warburg impedance (W), another name for the diffusion process, is a measurement of the impedance and resistance related to the solid-state diffusion of lithium ions in the electrode material. The state of charge (SoC), state of health (SoH), and electrode material characteristics are some of the variables that frequently affect the impedance caused by diffusion. A 45° slanted line at the low-frequency area of the Nyquist plot shown in figure 2.10 represents Warburg impedance. This line's slope indicates the diffusion process, and the impedance magnitude varies as the electrode materials' lithium diffusion coefficients do [63–65].

2.4.4.2.3 Monitoring State of Charge (SOC) and State of Health (SOH)

An effective technique for determining a battery's State of Health (SOH) and State of Charge (SOC) is Electrochemical Impedance Spectroscopy (EIS). With different SOC and SOH levels, the internal electrochemical processes of the battery change, and EIS provides insights into these processes by measuring the battery's impedance across a range of frequencies.

SOC is determined by dividing the battery's remaining charge by the maximum charge the battery is capable of delivering. As the battery charges or discharges, its impedance response changes due to variations in charge transfer resistance, double-layer capacitance, and diffusion properties, establishing a relationship between impedance and the State of Charge (SOC) [66]. Electrochemical Impedance Spectroscopy (EIS) captures this data, such as the real and imaginary parts of impedance, through Nyquist and Bode plots, which display distinct patterns corresponding to different SOC levels. These features provide valuable information that can be used to accurately model and estimate the SOC based on the observed impedance characteristics.

On the other hand, State of Health is as the ratio of the maximum charge of the battery to its rated capacity. Recently, it has been demonstrated that the SOH estimation method based on electrochemical impedance spectroscopy (EIS) works

well. A battery's aging and degeneration, which show up as variations in impedance, are reflected in its State of Health (SOH) [67]. Changes in Warburg impedance, decreased capacitance, and elevated internal resistance are some of the telltale signs of deteriorating battery health that emerge with time. Through the use of Electrochemical Impedance Spectroscopy (EIS) to measure impedance on a regular basis, these changes can be monitored and degradation factors such as capacity fading, loss of active material, or increased internal resistance can be identified, offering important information about the state of health of the battery [68–70].

Machine learning (ML) provides a sophisticated method for predicting the State of Charge (SOC) and State of Health (SOH) of batteries by using data-driven models that explain complex, nonlinear correlations in battery performance. Through the extraction of features from EIS data, these approaches are able to forecast the SOC and SOH with accuracy, which facilitates better tracking of performance, enhanced lifecycle management, and early detection of battery degradation. Machine learning methods, including Artificial Neural Networks (ANNs), Support Vector Machines (SVMs), and Convolutional Neural Networks (CNNs), analyse data such as voltage, current, temperature, and impedance to precisely predict state of charge (SOC) levels. For State of Health (SOH) estimation, models such as Long Short-Term Memory (LSTM) networks, Random Forests (RF), and Gradient Boosting Machines (GBM) evaluate features including cycle count, capacity decline, and impedance variations to determine battery deterioration. Two models for estimating the State of Health (SOH) of lithium-ion batteries (LIBs) using Electrochemical Impedance Spectroscopy (EIS) have been proposed where the first model enhances SOH estimation by employing an equivalent circuit model (ECM) and the second model leverages a convolutional neural network (CNN) integrated with bidirectional long short-term memory (BiLSTM), optimized by an improved Particle Swarm Optimization (IPSO) algorithm, offering a hybrid data-driven and optimization-based approach for precise predictions. The proposed models outperform traditional methods, showing up to a 94.8% improvement in prediction accuracy. These machine learning algorithms provide precise, flexible, and instantaneous estimation of state of charge (SOC) and state of health (SOH), rendering them indispensable for battery management in electric vehicles, energy storage systems, and consumer electronics [71–74].

2.5 METHODS FOR MEASURING THE CYCLIC VOLTAMMETRY OF LITHIUM ION BATTERY

There are several electrochemical analyses being researched to examine electrochemical processes. Chronoamperometry (CA), chronopotentiometry (CP), stripping voltammetry (SV), linear sweep voltammetry (LSV), and cyclic voltammetry (CV) are often employed electrochemical techniques [75–77]. It is feasible to determine the voltage at which oxidation or reduction takes place, as well as if contaminants are present or the reaction has proceeded correctly. In many different domains, but particularly in energy storage devices like Li ion batteries, these electrochemical evaluations are highly beneficial. A basic analytical approach among electrochemical techniques for a long time has been cyclic voltammetry. When compared to other metrics, CV has the following benefits: 1) The reversibility or irreversibility of the reactants' chemical reaction can be determined, 2) It is possible to ascertain the potential at which a reaction involving oxidation or reduction takes place, 3) It is also feasible to do quantitative analysis on compounds whose concentration is unknown, 4) It can be measured by adjusting test parameters including reactant concentration, temperature, and scan rate [78].

2.5.1 Principle of CV

Cyclic voltammetry is predicated on the linear sweep voltammetry principle, which makes use of a technology that measures current as the potential is swept linearly over time. The scan rate in this case is defined as the slope of the voltage change with time (ms^{-1}). The electrochemical reactivity of the materials, the scan rate for measurement, and the rate of electron transfer process all affect the data that LSV displays. Fig. 2.11 (a) describes how the LSV data are displayed as either a cathodic or anodic peak. Despite their close resemblance, CV does not terminate with a single sweep within a predetermined voltage range. When E2 is reached at the end, for instance, the voltage reverses back to E1, assuming that it ranges from E1 to E2. A "cyclic voltammogram," as illustrated in Fig. 2.11 (b), is a current against voltage plot that is referred to as such due to its characteristic. In the CV measurements, the scan rate (v) is the most crucial parameter. It shows the slope of a linear voltage change during the test and is swept from E1 to E2. The voltage, reversibility, and cyclability of redox processes can all be further elucidated by repeating many cycles under the same conditions. Furthermore, by varying the scan rate, it can be utilized to study the kinetics of electrochemical redox reactions.

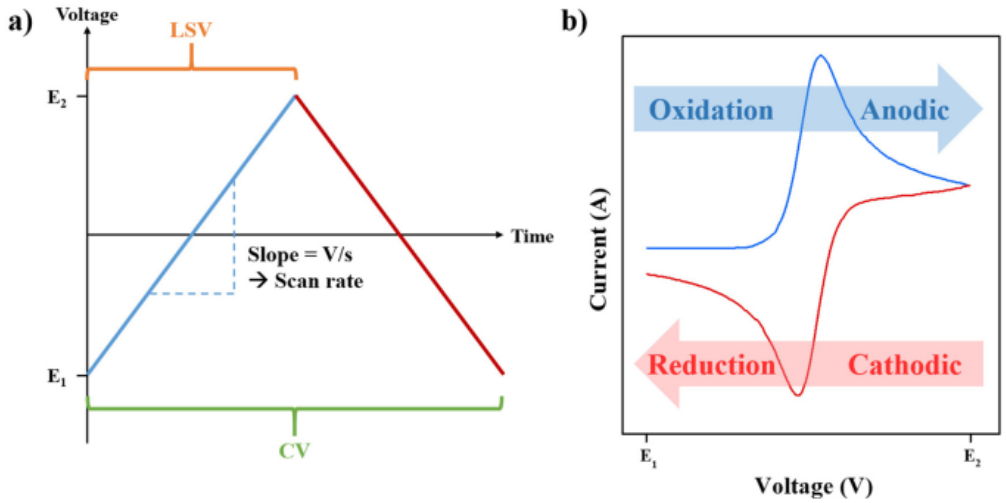

Figure 2.11 a) Linear sweep and cyclic voltammetry voltage vs. time profiles. b) A typical cathodic and anodic peak plot of a cyclic voltammogram [78].

2.5.2 *Parameters Influencing Voltammetric Curve Shape*

In cyclic voltammetry, a number of factors related to the electrochemical system, the experimental setup, and the electrode materials affect the form of a voltammetric curve. A thorough explanation of these parameters is discussed below:

2.5.2.1 Scan Rate

The shape of the voltametric curve is strongly influenced by the scan rate. Because of increased capacitance currents and diffusion constraints, peaks tend to spread and move with higher scan speeds, giving the impression that the redox reactions are less reversible. Slower scan rates, on the other hand, give the system more time to equilibrate, producing peaks that are sharper and more distinct [79].

2.5.2.2 Temperature

Ion mobility and reaction kinetics are directly affected by temperature. As electron transfer reactions speed up, higher temperatures enhance both, producing sharper peaks and less peak separation. Sluggish kinetics provide wider peaks and lower current densities at lower temperatures. The diffusion coefficient, which is essential for effective ion transport, is also improved by higher temperatures [80,81].

2.5.2.3 Concentration of Electroactive Species

Peak currents and curve clarity are directly impacted by the concentration of redox-active species. According to the Randles–Ševčík equation, higher concentrations produce greater peak currents, whereas lower concentrations produce weaker and less pronounced peaks. Electrochemical study has provided experimental validation for this association [82].

2.5.2.4 Solution Resistance (Ohmic Drop)

The voltammetric curve is greatly impacted by solution resistance, which introduces an uncompensated voltage loss that causes distorted and widened peaks. One of the most frequent problems in electrochemical cell design is high resistance, which is frequently brought on by low electrolyte conductivity [83].

2.5.2.5 Diffusion and Convection

The shape of the curve is mostly determined by mass transport processes, especially diffusion and convection. While convection, such as stirring, alters the equilibrium and broadens the peaks, diffusion-dominated systems show distinct, sharp peaks. These effects have been measured in controlled experiments [84].

2.5.2.6 Reversibility of the Reaction

Irreversible systems have wider, asymmetric peaks because of slower electron transfer kinetics, whereas reversible systems produce symmetric redox peaks with tiny peak separations. Using conventional electrochemical theory and experimentation, the reversibility of reactions can be evaluated [85].

2.5.2.7 Capacitance of the Double Layer

In cyclic voltammetry, the baseline current is impacted by the double-layer capacitance. The redox peaks are obscured and the curve form is changed by a large capacitance, which is frequently connected to rough electrodes or concentrated electrolytes. Strategies to reduce these impacts for more understandable data interpretation have been investigated in research [86].

2.6 LITHIUM PLATING IN LITHIUM-ION BATTERIES

A crucial process that happens when lithium-ion batteries are being charged is called lithium plating, which results in the deposition of metallic lithium on the anode surface. Battery longevity, safety, and performance are all negatively impacted by this phenomenon.

Both the anode Li plating and the Li interaction into active materials occur simultaneously during the charging process, as seen in equation 16 and 17 [87].

$$xLi^+ + Li_\delta C_\delta + xe^- \rightarrow Li_\delta C_\delta \tag{16}$$

$$yLi^+ + ye^- \rightarrow yLi \tag{17}$$

Li plating current and intercalation current split the overall charging current under these circumstances. As charging continues, the charge current for Li intercalation eventually decreases because of the limited solid-state diffusion in graphite and the declining vacancy sites for Li intercalation. At the same time, the current for Li plating goes up since the electrolyte's transport rate of Li+ is higher than the Li-intercalation rate. This causes more Li+ to accumulate on the surface and lowers the anode potential to less than 0 V shown in Fig. 2.12 (a).

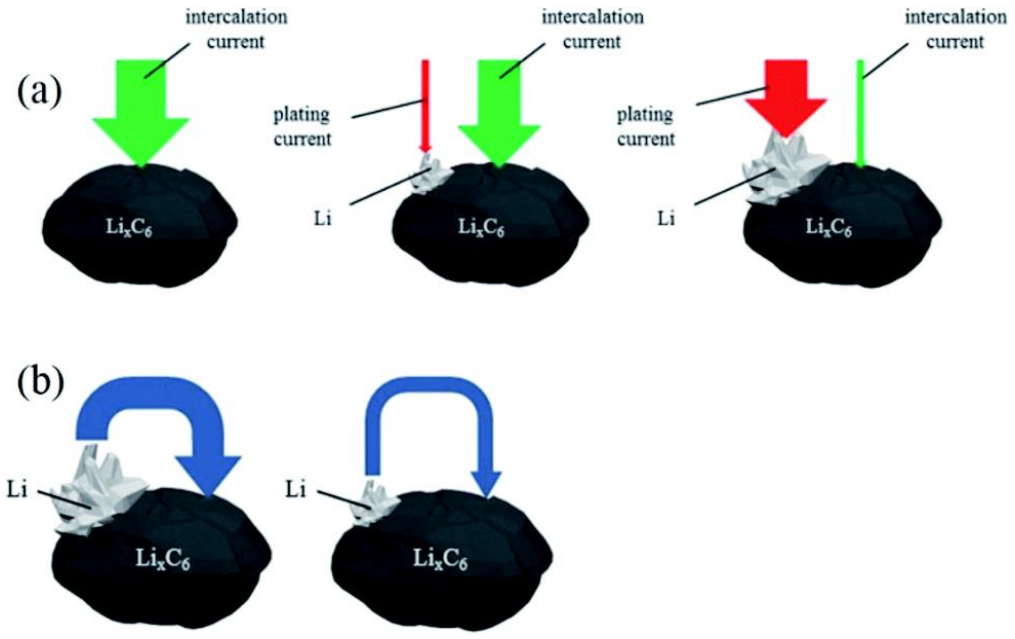

Figure 2.12 Illustration of (a) the plating and intercalation currents during charging to higher charge states and (b) the re-intercalation of deposited lithium between rest periods [87]

A part of the deposited lithium may experience two further reactions when anode lithium plating takes place, regardless of any external current. One is reinsertion into the graphite anode during the tapering charging or resting phase shown in equation 18, and the other one is reaction with the electrolyte shown in equation 19.

$$\varepsilon Li + Li_{\delta+x}C_6 \rightarrow Li_{\delta+x+\varepsilon}C_6 \quad (18)$$

$$R + Li \rightarrow R - Li \quad (19)$$

Where, R is electrolyte

At the anode, two reactions may occur one after the other during discharge [87]:

$$Li \rightarrow Li^+ + e^- \quad (20)$$

$$Li_{\delta+x+\varepsilon}C_6 \rightarrow 6C + (\delta + x + \varepsilon)Li^+ + (\delta + x + \varepsilon)e^- \quad (21)$$

The reinsertion current of deposited Li during relaxation or tapering charge is clearly visible in Fig. 2.12 (b). A potential difference between the deposited Li and the Li_xC_6 in the graphite bulk is present when lithium deposits on the graphite surface. If enough time is allowed, the potential difference forces the deposited Li to re-insert into the graphite until the inserted active Li or potential difference vanishes. The amount of deposited Li determines the reinsertion current; hence, the more deposited Li, the more reinsertion takes place during relaxation. Reversible deposited lithium is defined as lithium that undergoes no capacity loss due to re-intercalation (eqn. 18) and Li stripping (eqn. 21) processes. Nevertheless, deposited lithium reacts with the electrolyte to generate surface coatings, which causes irreversible capacity loss.

2.6.1 Challenges with Anode Lithium Plating

Anode lithium plating's negative consequences on LIBs mostly include safety concerns and quick performance deterioration. Because metallic lithium is thermodynamically active in polar aprotic solvents, when anode lithium plating takes place during abnormal charging, the deposited metallic lithium spontaneously combines with the electrolyte until an intact passivation layer, or solid electrolyte interphase (SEI) film, forms [88]. Poor coulombic efficiency and capacity deterioration are caused by the reaction between metallic lithium and the electrolyte, which consumes the active lithium and electrolyte. Concurrently, as the Li ions

intercalate and deintercalated, the generated SEI layer causes further polarization by raising the internal resistance of LIBs [89]. After anode lithium plating, partially plated lithium, particularly dendritic lithium, may lose electrical contact with the anode and, in the event of a subsequent discharge, may potentially create floating shards or structures in the electrolyte (referred to as dead lithium). Both dead lithium and the development of SEI film cause rapid capacity deterioration during anode lithium plating and will lead to the permanent loss of active lithium. Because the reaction of metallic Li with electrolyte causes the SEI film to thicken and the electrolyte to dry up, anode lithium plating is a self-accelerating process [90,91].

Anode lithium plating can lead to safety problems such as internal short circuits from the dendritic lithium and thermal runaway from the strong exothermic interaction between the electrolyte and the deposited lithium. Lithium deposits are frequently found as needles or dendrites that resemble the dendrites of the metal Li electrode. As a result, the dendrites in LIBs and lithium metal batteries have similar negative impacts on cell safety. Dendritic lithium production is intimately associated with the concentration of Li+ ions on the anode surface, the charge current, and the SEI film [92–94].

An additional safety concern is that the deposited lithium speeds up the thermal runaway of LIBs, even when it is not in dendritic form. The quick exothermic interaction between the electrolyte and the deposited lithium will generate a lot of heat, raising the cell temperature and potentially igniting or exploding LIBs [95,96].

2.6.2 Morphology Characterization Techniques

Characterizing the morphology of dendritic lithium on scales ranging from millimeters to nanometers has been made possible by in situ and ex situ optical microscopy, SEM, and TEM. These methods also offer qualitative insights into the mechanism of anode lithium plating, which is useful in identifying effective strategies to stop lithium dendrite growth. Due to its easy design, optical microscopy is typically used for in situ observation of anode lithium plating. On a macro scale, in situ optical microscopy has been used extensively to monitor the dendritic lithium development process on metal lithium or inert electrodes. Due to graphite's great absorption of visible light, only significant amounts of dendritic Li can be seen; most optical investigations of graphite are dependent on color shifts [97–99]. Guo et al [100] used an optical graphite/$LiFePO_4$ cell to examine changes in the dendrites of lithium in situ. The graphite turned golden after ten minutes of overcharging; the lithium deposition on the graphite electrode's edge was visible and become more noticeable as the overcharge period increased.

Chapter 3

Methodology

3.1 INTRODUCTION

The tasks were executed in the sequence outlined in Fig. 3.1, and the investigation focused on examining the cyclic performance as well as the internal resistance of Li-ion battery cells.

3.2 RESEARCH FLOWCHART

Figure 3.1 outlines the steps followed to complete this study. The experiment began with connecting the battery cell to the LAND battery testing system to assess its cyclic performance. Next, Electrochemical Impedance Spectroscopy (EIS) and Cyclic Voltammetry (CV) were employed to measure the battery's internal resistance and cyclic voltammogram. Afterward, the battery was disassembled, and the anode surface was examined using an optical microscope. Finally, the collected data were analyzed through plotted graphs, and a comparative evaluation was performed.

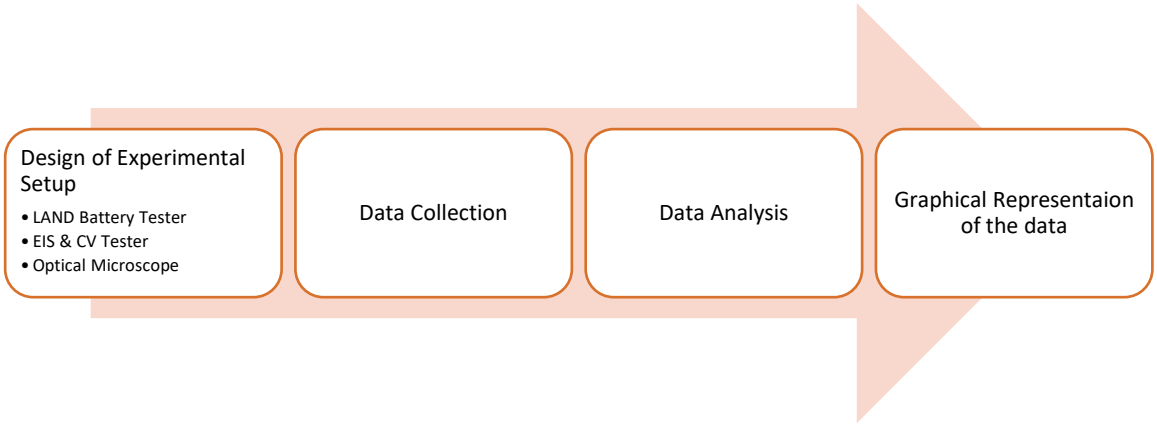

Figure 3.1 Work flow chart

3.3 LIST OF EQUIPMENTS

The list of necessary instruments for the experiment along with their intended uses showed in Table 3.1.

Table 3.1 Equipment lists and their purpose of use

Instrument	Purpose
600mAh pouch cell	To investigate the cyclic performance, internal resistance and the surface morphology of the battery's anode
LAND Battery testing system	To charge and discharge a battery cell
Desktop Computer	To get the data from the LAND Battery testing system
EIS tester	For evaluating internal resistance of battery
CV tester	For conducting cyclic voltammogram test of battery
Optical Microscope	For observing the anode material's surface flaws, scratches, fractures, and irregularities
Hot plate	To create a high temperature environment
Thermometer	To measure the temperature
Multimeter	To measure the voltage
Glass box	To maintain a constant temperature
Wire	To connect the battery with the holder and the LAND Battery testing system.

3.3.1 Battery

A 600mAh pouch Li-ion battery shown in Fig. 3.2, which is a lightweight and compact energy storage device widely utilized in portable electronics and experimental research. The pouch design provides a high energy density and flexibility, making it suitable for applications requiring compact and efficient power sources.

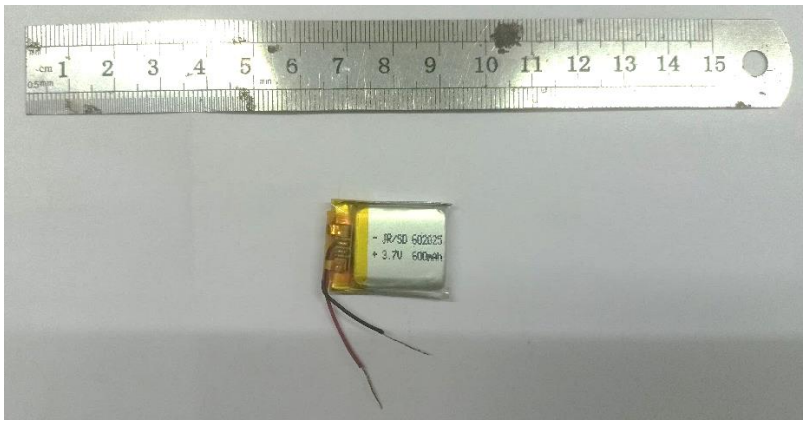

Figure 3.2 Pouch cell

3.3.2 Battery Tester

The battery's electrochemical properties were examined using a battery tester, as seen in Fig. 3.3. By monitoring the behavior of the cells during cycles of charge and discharge, a battery cycler evaluates the battery's performance. During battery cycling, a number of factors can be evaluated, such as capacity, battery efficiency, and self-discharge. The multichannel LANHE LAND-CT2001A battery testing equipment was used to conduct the test in the voltage range of 0.2 V to 3.7 V.

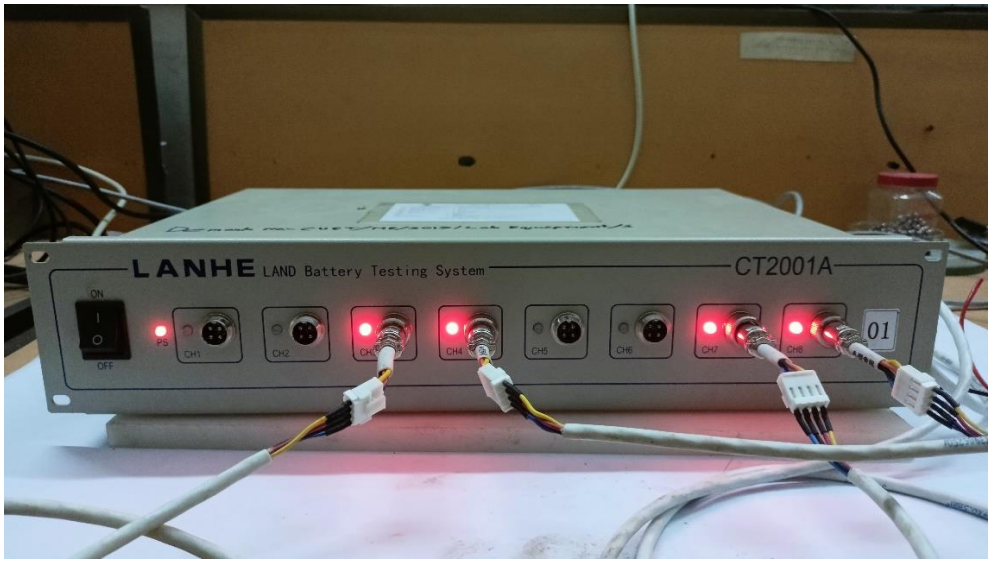

Figure 3.3 LAND battery testing device

Figure 3.4 shows the schematic and the real connection of the battery with the testing device, where the big clips for current input/output and the little clips for voltage

measurement. Red clips are connected with the positive terminal of a battery and the black clips are connected with the negative terminal of the battery.

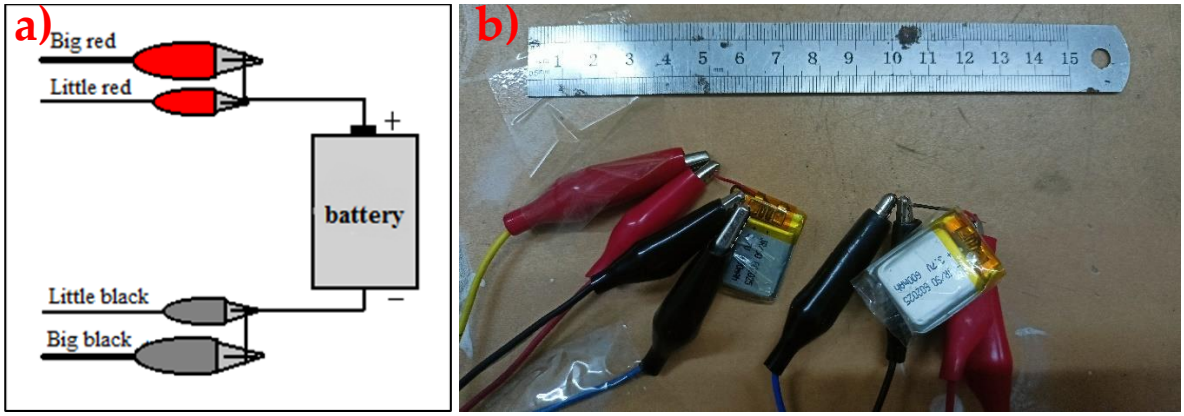

Figure 3.4 Battery wire connection (a) Schematic diagram [101] (b) Real connection

3.3.3 EIS and CV Tester

CORRTEST CS100 device, shown in Fig. 3.5, which is a precision electrochemical workstation designed for advanced electrochemical testing and analysis. It is widely used in research and industrial applications, particularly for evaluating the electrochemical properties of materials, corrosion behavior, and energy storage systems like batteries and fuel cells. The device is equipped with a powerful control system and high-resolution measurement capabilities, making it suitable for a wide range of electrochemical techniques. In our experiment, the pouch cell's cyclic voltammogram and EIS were tested using a CORRTEST CS100 device

Figure 3.5 EIS and CV testing device

3.3.4 *Optical Microscope*

An optical microscope shown in Fig. 3.6 was used for investigating the pouch cell's anode surface morphology.

Figure 3.6 Optical microscope

3.3.5 *Magnetic Stirrer with Hot Plate*

In order to raise the temperature, a 78-1 model magnetic stirrer with a hot plate was employed. The magnetic stirrer model utilized in this investigation is depicted in Fig. 3.7.

Figure 3.7 Hot plate

3.3.6 Thermometer

A mercury (Hg) thermometer is a kind of liquid-in-glass thermometer that is frequently used to measure temperatures precisely shown in Fig. 3.8. In order for mercury thermometers to work, mercury inside a sealed, calibrated glass tube must expand and contract in response to temperature variations. Because of its high boiling point and stable thermal expansion characteristics, mercury is a great option for precise and trustworthy temperature readings across a broad range. In our experiment we used thermometer to measure the temperature during the cycling of the battery.

Figure 3.8 Thermometer

3.3.7 Multimeter

A multimeter is a multipurpose electrical device that can be used as an ohmmeter, voltmeter, and ammeter, as shown in Fig. 3.9. It has both positive and negative reading indication needles and a numeric LCD digital display. Motors, batteries, and power sources are among the electrical components that are frequently tested with multimeters. Multiple electrical properties, such as voltage, current, resistance, and other factors including continuity, capacitance, and temperature, can be measured by a multimeter, which combines the capabilities of several measurement tools into a single, small gadget. We measured the open-circuit voltage of the battery in our experiment using a multimeter.

Figure 3.9 Multimeter

3.4 EXPERIMENTAL SETUP

Three distinct experimental setups were utilized for the battery cycling, Electrochemical Impedance Spectroscopy (EIS) and Cyclic Voltammetry (CV) testing, and surface morphology analysis. Each setup was designed to focus on a specific aspect of the battery's performance, providing comprehensive insights into its behavior under various conditions.

3.4.1 Experimental Setup for Battery Cycling

Figure 3.10 illustrates the schematic diagram of the experimental setup. At the very beginning of the experiment, the data was taken at room temperature. Then, the heater was switched on to create an environment above the room temperature to take data at 100˚C. The heater was enclosed with a glass box to maintain a constant temperature. To measure the temperature a thermometer was set near the battery. Batteries charging and discharging were controlled by the LAND Battery testing system. And the LAND battery testing system was controlled by the software known as LANDmon v5.9K. For data visualization, LANDdt v5.9K was used.

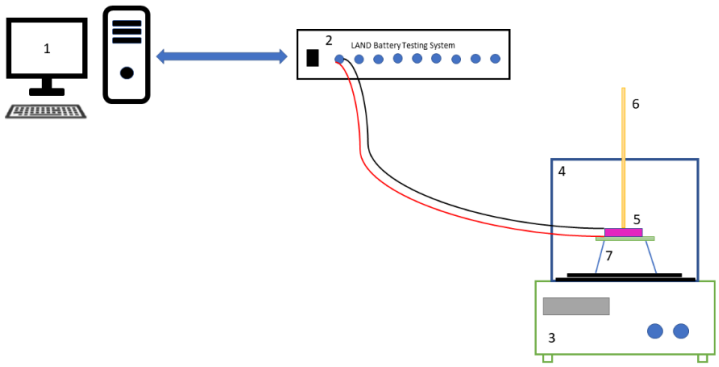

Figure 3.10 Diagrammatic representation of the battery cycling experimental setup

1 Desktop Computer
2 LAND Battery Testing System
3 Magnetic Stirrer with a hot plate
4 Glass box
5 Li-ion Battery
6 Thermometer
7 Stand

The algorithm used for charging and discharging cycle in the LANDmon software is illustrated in Fig. 3.11

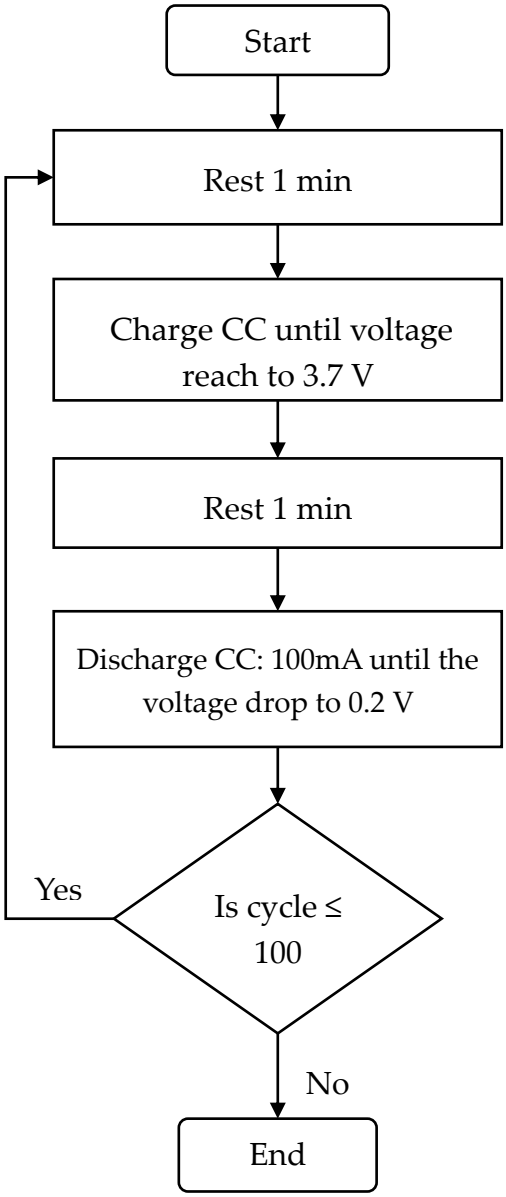

Figure 3.11 Algorithm for charging and discharging

The experimental setup used to conduct this study is shown in Figure 3.12. The cell was at 100˚C when the setup photo was shot. To keep the temperature around the battery cell consistent, a glass a box was built. A thermometer was used to measure the battery's and the surrounding air's temperatures.

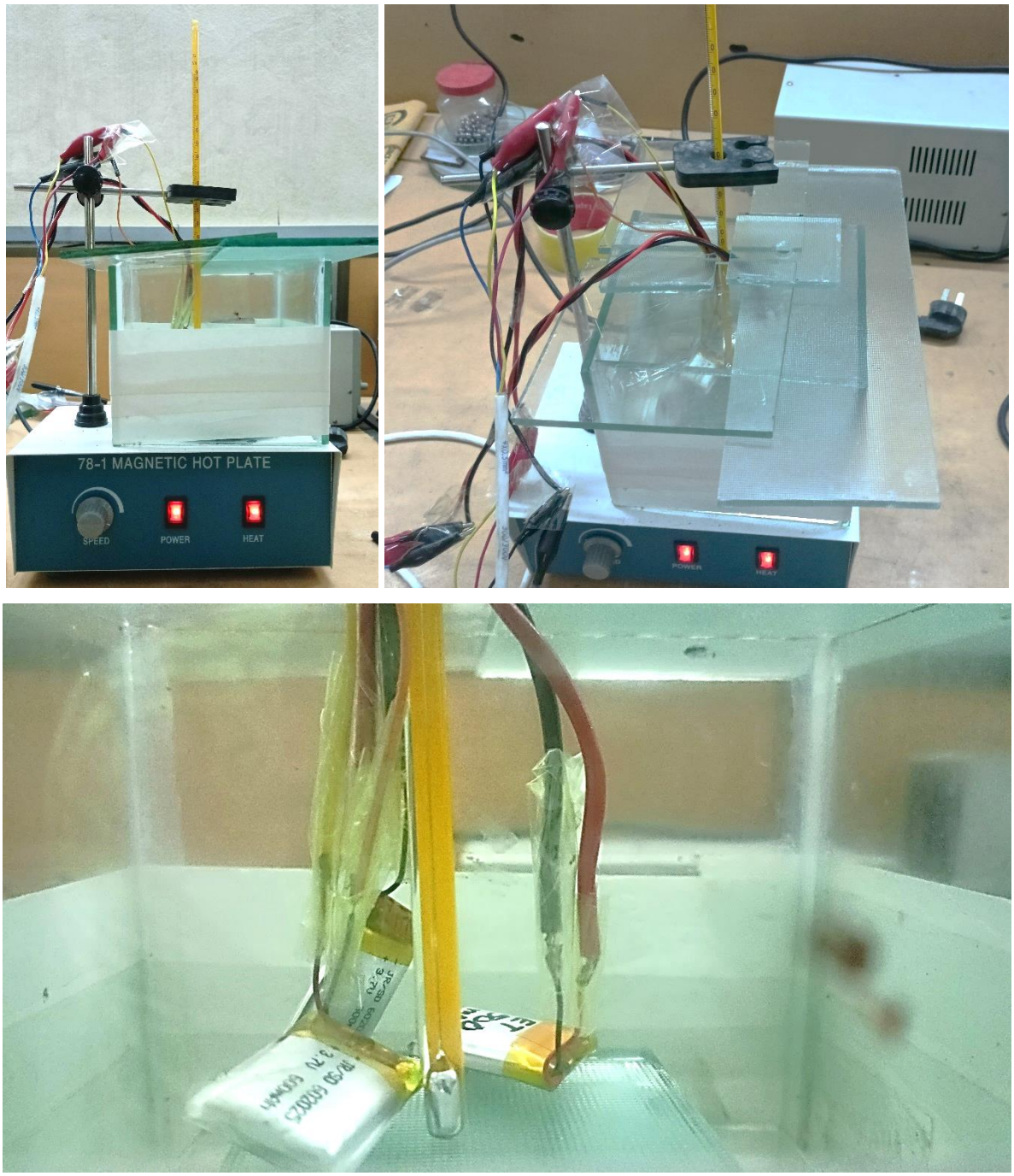

Figure 3.12 Experimental setup at lab for battery cycling

3.4.2 Experimental Setup for EIS and CV

To conduct Cyclic Voltammetry (CV) and Electrochemical Impedance Spectroscopy (EIS) testing on the battery, an experimental setup was created utilizing the CORRTEST CS100 shown in Fig. 3.13. With the help of the CORRTEST CS100, the battery's electrochemical properties could be precisely measured. The data gathered was shown in real time on a computer screen that was linked. With the use of this configuration, the battery's internal resistance and cyclic voltammetry behavior could be thoroughly examined, yielding important information on its electrochemical characteristics and overall performance. The data obtained from the CORRTEST CS100 during the EIS and CV experiments were analyzed using ZView software. This powerful tool allowed for precise fitting and interpretation of the impedance spectra and cyclic voltammetry results, enabling a deeper understanding of the battery's electrochemical behavior and internal resistance characteristics.

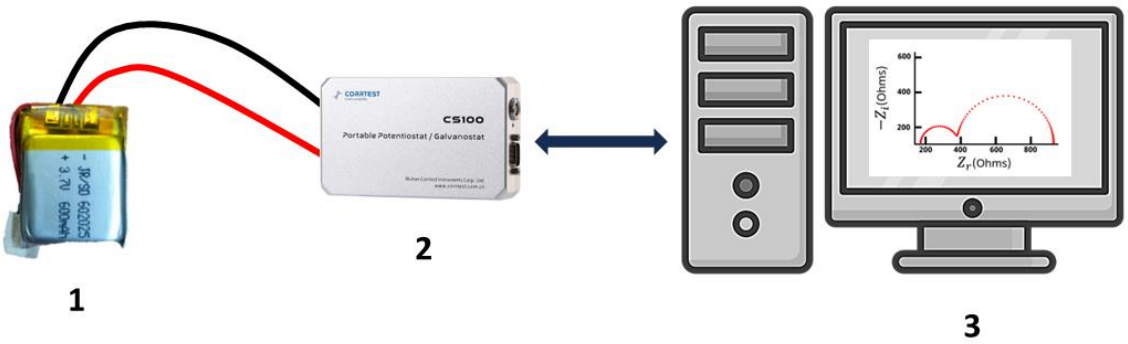

Figure 3.13 Diagrammatic representation of the battery's EIS and CV experiment

1 Lithium-ion Battery
2 CORRTEST CS100
3 Desktop Computer

3.4.3 Experimental Setup for Optical Microscopy

A pouch cell is fabricated by enclosing stacked or rolled electrodes within an aluminum-laminated plastic pouch. This pouch acts as a flexible and lightweight outer casing, protecting the internal components while allowing efficient packaging of the cell. During the disassembly process shown in Fig. 3.14, the pouch was carefully cut open using scissors to access the internal components. Special attention was given to ensure precision during the cutting process to avoid damaging the electrodes or separator inside. Once the pouch was opened, the rolled electrode assembly was gently extracted and separated for further analysis.

Figure 3.14 Steps of battery disassembly

A digital optical microscope was used to build an experimental setup for observing and examining the battery's anode surface shown in Fig. 3.15. A computer screen that was attached to the microscope showed real-time, high-resolution pictures of the anode. This configuration allowed for a thorough analysis of the surface morphology, which offered important information on the structural alterations and possible deterioration of the anode material over the period of battery operation. The computer's connection with the digital microscope made it easier to see and record the experimental data precisely.

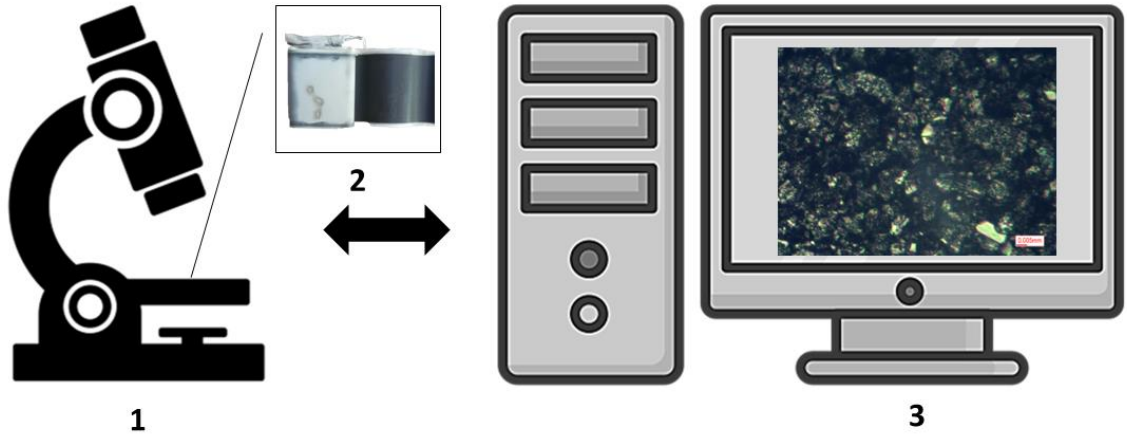

Figure 3.15 Diagrammatic representation of the battery’s anode surface observation

1 Optical Microscope
2 Anode Material of the LIB
3 Desktop Computer

Chapter 4

Results and Discussions

4.1 INTRODUCTION

The main findings from experimental investigations are presented in this chapter, which forms the basis of the study. Their consequences for the performance of lithium-ion batteries are also examined. This chapter attempts to close the gap between observed occurrences and underlying mechanisms by methodically examining the data, offering a thorough comprehension of the study's goals.

To clarify the structural, electrochemical, and thermal behaviors of the lithium-ion battery components, the outcomes of methods including optical microscopy, cyclic performance testing, and electrochemical impedance spectroscopy (EIS) are carefully examined. Finding patterns, comparing results under various experimental settings, and connecting these results to theoretical predictions and previous research are the main goals of each dataset's interpretation. The evolution of surface shape, capacity retention, coulombic efficiency, and resistance variations during cycling are among the main performance parameters that receive particular attention. The implications of different current rates and temperatures are examined in relation to these findings, emphasizing how they affect battery degradation processes such electrolyte degradation and SEI layer formation.

4.2 ELECTROCHEMICAL ANALYSIS

Figures 4.1 and 4.2, respectively, depict the changes in voltage and current with time over (a) 1-30, (b) 31-60, and 61-100 galvanostatic Charge-Discharge cycles.

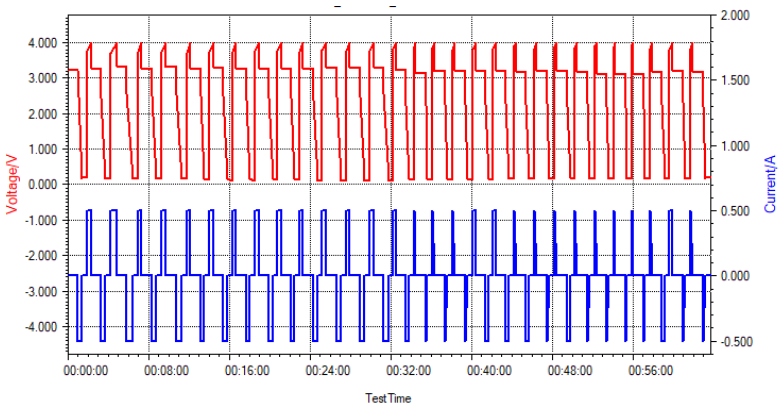

Figure 4.1 Change of current and voltage with respect to time for 1-30 charge discharge cycles

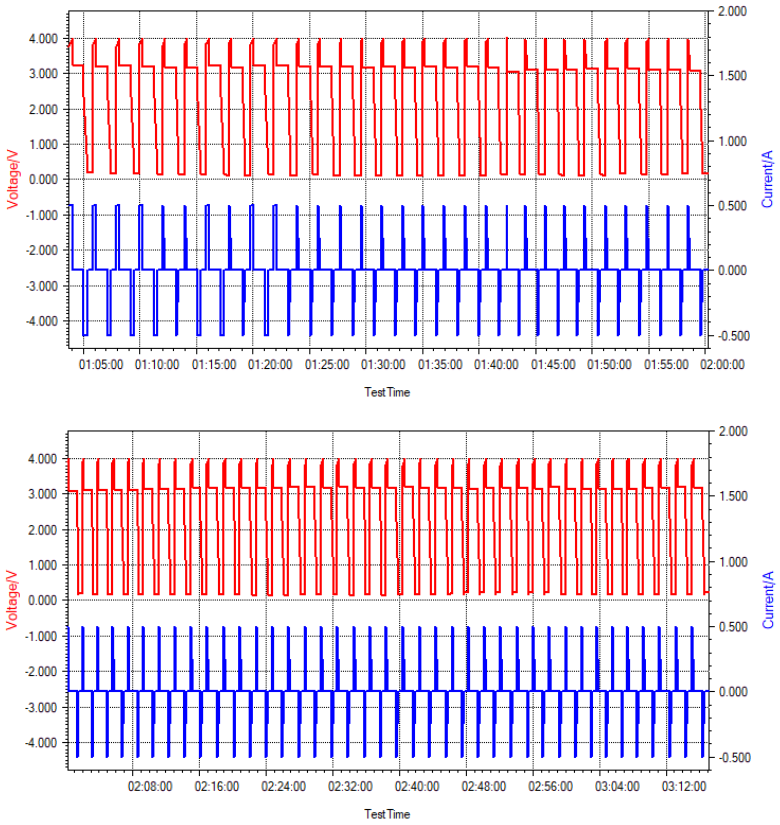

Figure 4.2 Change of current and voltage with respect to time for (a) 31-60 charge discharge cycles (b) 61-100 charge discharge cycles

Figure 4.3 illustrates the cycling performance of the battery, showing that the initial capacities are relatively high and stable during the first few cycles. However, a gradual decline in capacity is observed over 100 cycles, indicative of capacity fading. This degradation can be attributed to factors such as the formation of the Solid Electrolyte Interphase (SEI), side reactions, and electrolyte decomposition. The Coulombic Efficiency (CE) starts near 100%, reflecting efficient charge and discharge processes in the early cycles. A slight decrease in CE over subsequent cycles suggests an increase in irreversible reactions or lithium loss within the cell, contributing to the overall decline in performance.

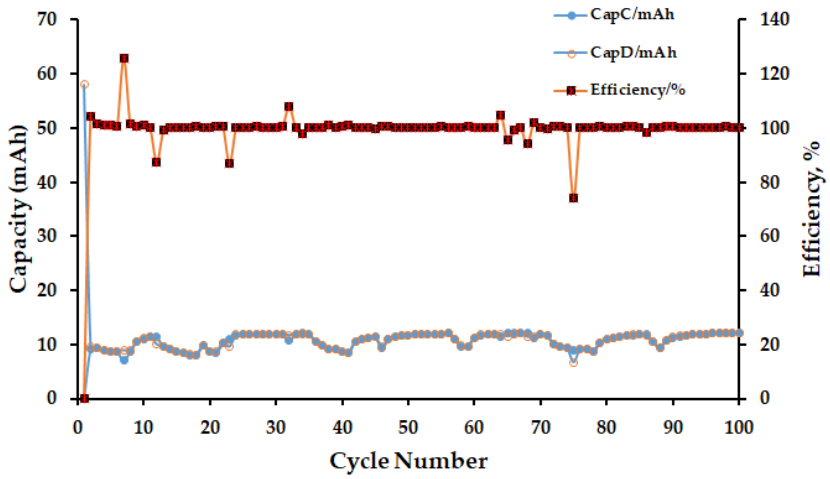

Figure 4.3 Cyclic performance of the battery at a current rate of 100mA under room temperature conditions

At room temperature, cycling the battery at 300mA revealed irregularities in Coulombic Efficiency (CE) during cycle numbers 48 and 96 shown in Fig. 4.4. Notably, the CE spiked unexpectedly, reaching 300% and 240% for these cycles, respectively. Such anomalous peaks are indicative of abnormal behavior within the battery, likely caused by an internal short circuit. Internal short circuits can occur due to several factors, such as the growth of dendrites, mechanical damage to the separator, or degradation of internal components. These events cause unintended direct pathways for current flow, leading to abnormal charge/discharge dynamics. The sudden spikes in CE suggest that the battery temporarily exhibited uncontrolled discharge behavior, releasing stored energy rapidly and skewing the charge-discharge efficiency calculation [102].

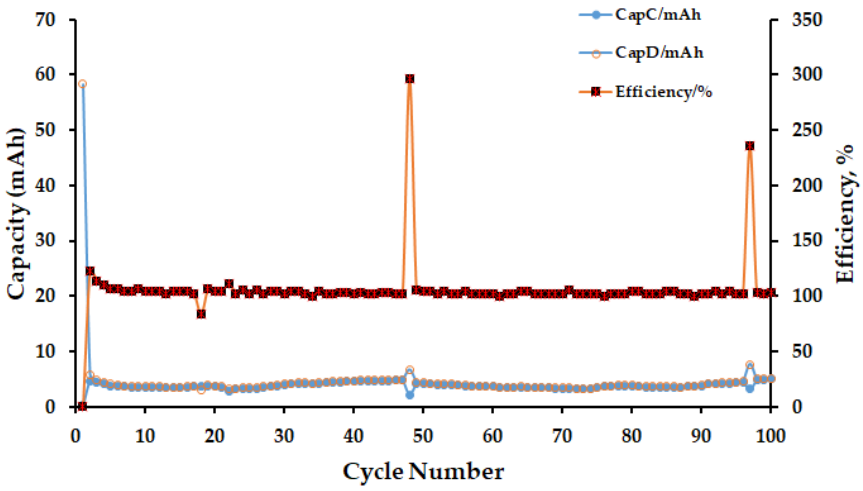

Figure 4.4 Cyclic performance of the battery at a current rate of 300mA under room temperature conditions

Figure 4.5 illustrates the cyclic performance of the battery at room temperature under a constant current of 300mA. Over 100 cycles, the charging and discharging capacities remained relatively stable, with the exception of the first cycle. The initial capacity was significantly high at around 120mAh but dropped drastically after the first cycle, stabilizing in the range of 5 to 8mAh. This substantial decline could be attributed to the lithium ions being unable to fully migrate between the electrodes due to the high current rate, leading to limited intercalation and deintercalation processes during rapid charge-discharge cycles.

An anomaly was observed during the 76th cycle, where the Coulombic Efficiency (CE) spiked unexpectedly to approximately 325%. Such a sudden increase in CE suggests the occurrence of an internal short circuit within the battery. This malfunction likely caused an uncontrolled current flow, bypassing the normal electrochemical pathways, and resulted in an inflated CE value. These findings highlight the impact of fast cycling on battery stability and the potential risks of internal failures during high-rate operation.

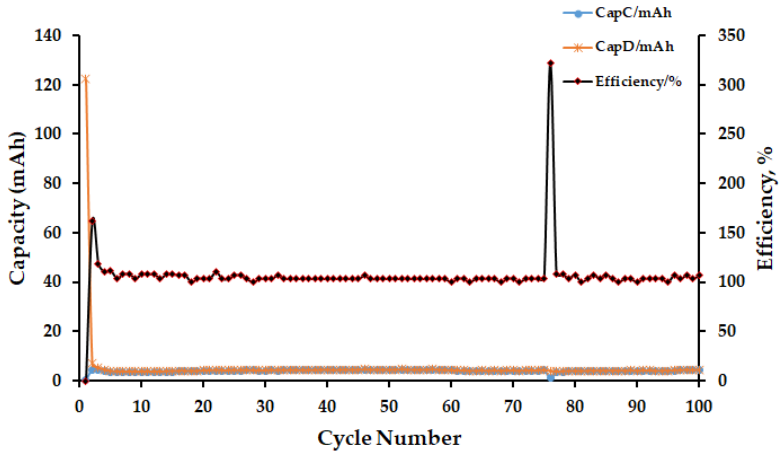

Figure 4.5 Cyclic performance of the battery at a current rate of 500mA under room temperature conditions

Figure 4.6 illustrates the cyclic performance of the battery when cycled at 100°C with a 100mA current. Under these conditions, the battery exhibited abnormal behavior, with charging and discharging capacities fluctuating significantly over the course of 100 cycles. This instability suggests that the battery was undergoing degradation or experiencing internal processes that hindered consistent performance.

As a result of these fluctuations, the Coulombic Efficiency (CE) also oscillated throughout the cycles, ranging between 80% and 120%. Such oscillations in CE indicate irregular charge/discharge behavior, potentially caused by factors like

electrolyte degradation, side reactions, or thermal effects on the internal components. The high temperature likely accelerated these issues, causing variations in the electrochemical reactions within the battery.

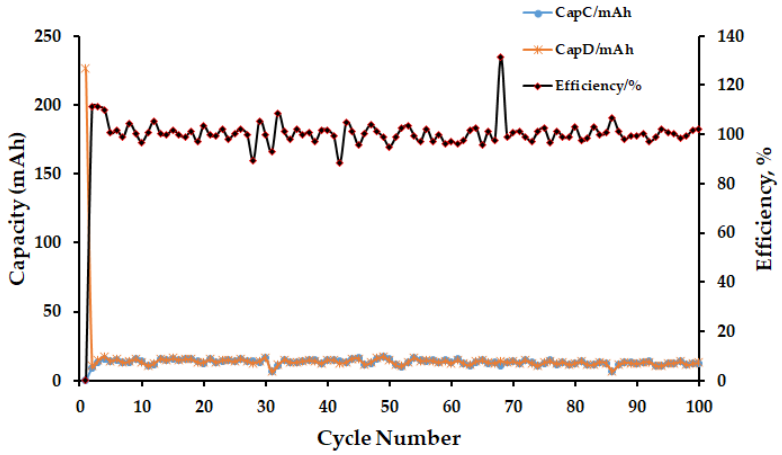

Figure 4.6 Cyclic performance of the battery at a current rate of 100mA under 100˚C temperature conditions

Figure 4.7 illustrates the cyclic performance of the LIB at 100°C under a constant current of 300mA. The charging and discharging capacities exhibited no noticeable pattern, highlighting significant instability under these extreme conditions. The maximum capacity observed was approximately 6mAh during the 20th cycle. However, the capacity dropped sharply to its lowest point of around 1mAh at the 50th cycle. Following this minimum, the capacity fluctuated over the next 50 cycles, eventually stabilizing at approximately 3mAh by the 100th cycle.

The Coulombic Efficiency (CE) mirrored the instability of the charging and discharging capacities, fluctuating throughout the cycling process. The highest CE, approximately 130%, was observed during the 50th cycle, coinciding with the capacity's steep decline. Such behavior indicates significant inefficiencies and potential side reactions, likely exacerbated by the high temperature and current, which accelerate degradation mechanisms such as electrolyte decomposition and loss of active material.

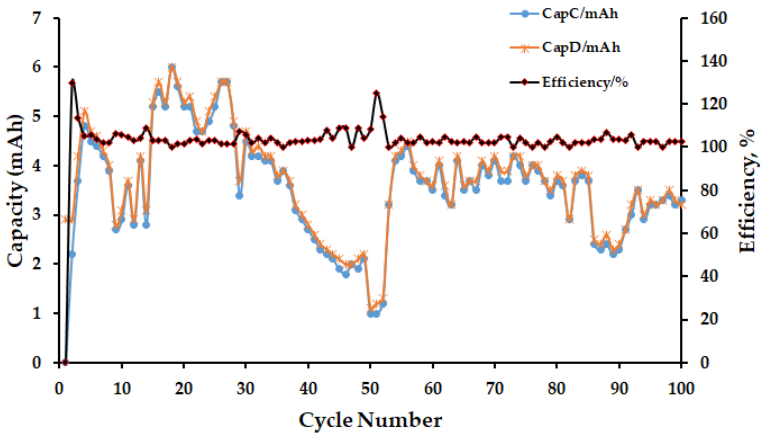

Figure 4.7 Cyclic performance of the battery at a current rate of 300mA under 100˚C temperature conditions

The worst cycling performance was observed when the battery was operated at 100°C under a constant current of 500mA shown in Fig. 4.8. Both the charging and discharging capacities exhibited a fluctuating downward trend, starting at 5mAh and decreasing to approximately 2mAh after 100 cycles. The capacity fading can be attributed to several factors. One primary cause is the formation of the Solid Electrolyte Interphase (SEI) layer, which consumes active lithium and electrolyte. Additionally, the high current rate may have prevented lithium ions from adequately migrating between electrodes during fast charging, leading to inefficient intercalation. Another contributing factor could be the formation of lithium plating, which not only depletes active lithium but also increases internal resistance and poses safety risks.

As a consequence of these degradation mechanisms, the Coulombic Efficiency (CE) showed irregular behavior throughout the 100 cycles. For most cycles, the CE exceeded 100%, with a peak of approximately 150% during the 50th cycle, coinciding with the lowest capacity values. Such anomalies in CE suggest significant inefficiencies and potential internal short circuits caused by rapid cycling at elevated temperatures.

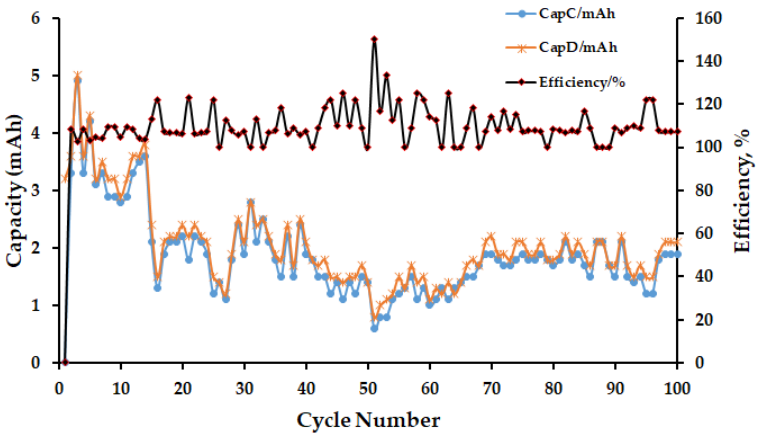

Figure 4.8 Cyclic performance of the battery at a current rate of 500mA under 100˚C temperature conditions

Figures 4.9 and 4.10 illustrate the EIS data for the pouch cell cycled at room temperature and at 100°C, respectively. In both cases, the impedance of the battery before cycling was significantly higher compared to the conditions after cycling at 100 mA, 300 mA, and 500 mA. This high initial impedance is attributed to the incomplete formation and stabilization of the solid electrolyte interphase (SEI) layer, as well as suboptimal electrolyte wetting and electrode interfaces. After cycling, the impedance decreases due to the stabilization of the SEI layer, improved electrode activation, and enhanced electrolyte redistribution, which collectively optimize the ionic and charge transport pathways. The graphs also reveal similar impedance behavior within a specific range for all three current densities, indicating that the battery operates within an optimal electrochemical window, with minimal polarization effects and stable charge transfer and ion diffusion processes at these cycling currents.

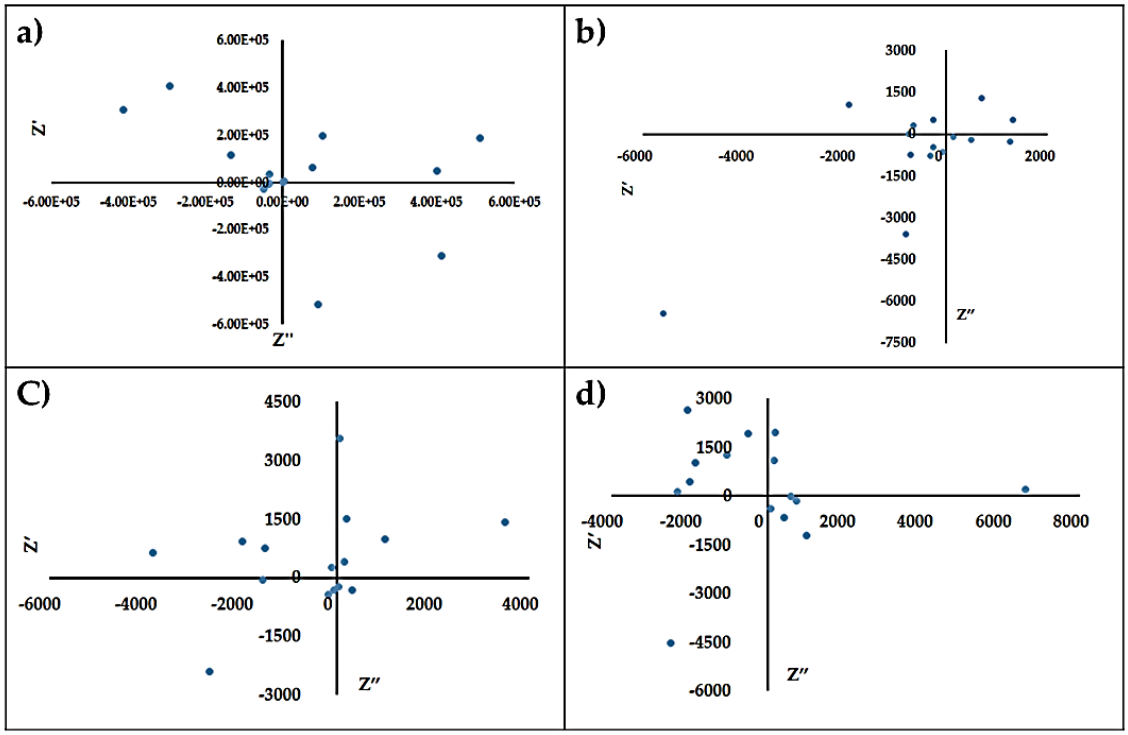

Figure 4.9 EIS data at room temperature a) Fresh cell b) After 100th cycle at 100 mA current rate c) After 100th cycle at 300 mA current rate d) After 100th cycle at 500 mA current rate

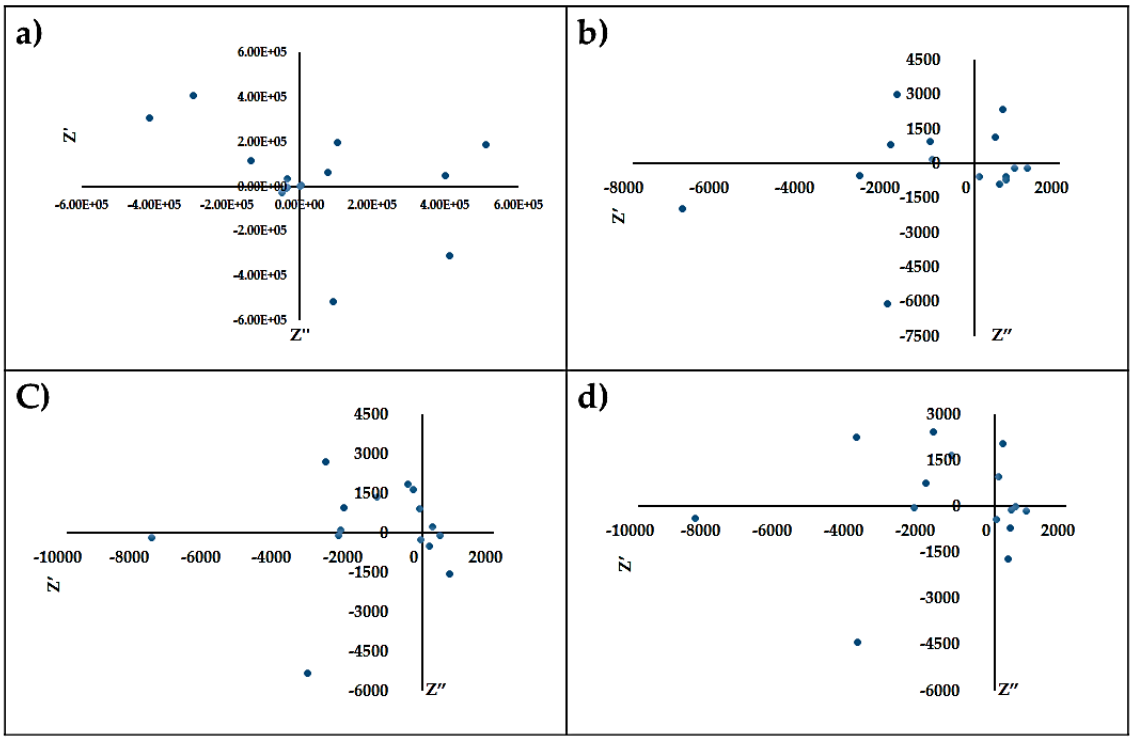

Figure 4.10 EIS data at 100˚C temperature a) Fresh cell b) After 100th cycle at 100 mA current rate c) After 100th cycle at 300 mA current rate d) After 100th cycle at 500 mA current rate

The cyclic voltammetry (CV) graphs illustrate the electrochemical behavior of a lithium-ion battery (LIB) at room temperature (Figure 4.11) and 100˚C (Figure 4.12) under varying conditions. For both temperatures, the fresh cell exhibits redox peaks corresponding to lithium intercalation and deintercalation, though these are less defined at room temperature due to an undeveloped SEI layer and inactive electrode surfaces. After 100 cycles at 100 mA, the redox peaks become sharper and more pronounced, indicating improved reaction kinetics and reduced resistance as the SEI stabilizes and the electrode activates. At higher currents (300 mA and 500 mA), the peaks show increased current densities but become broader, with greater peak separation at 500 mA due to polarization and resistance effects.

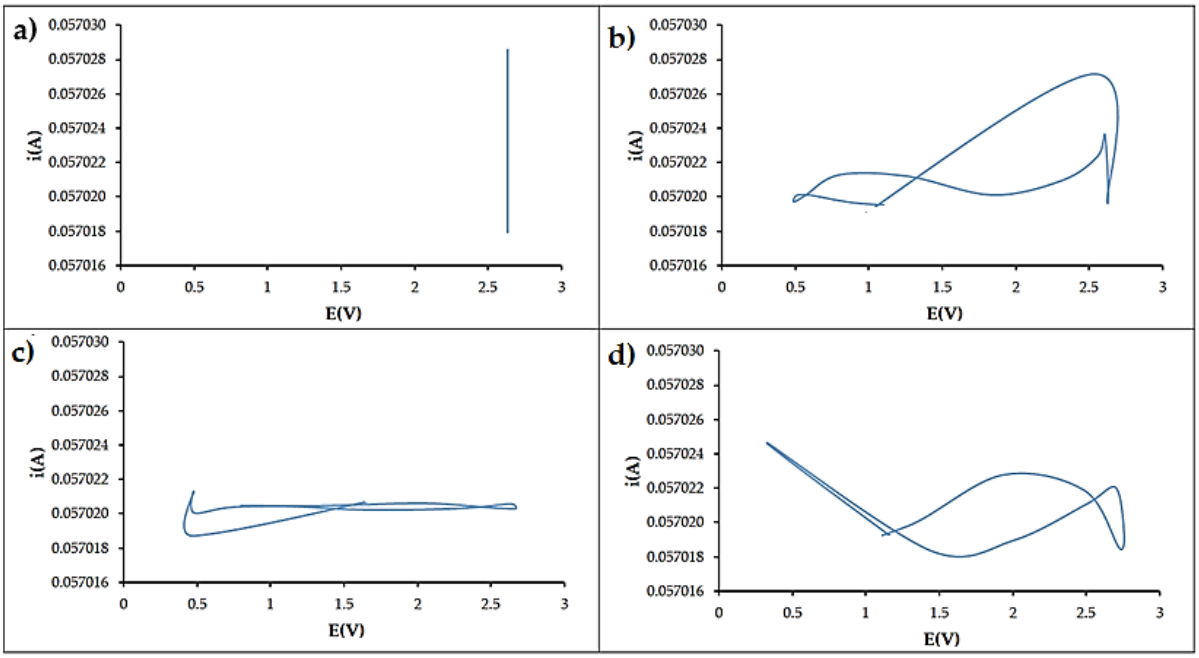

Figure 4.11 CV at room temperature a) Fresh cell b) After 100th cycle at 100 mA current rate c) After 100th cycle at 300 mA current rate d) After 100th cycle at 500 mA current rate

Elevated temperature significantly enhances reaction kinetics and ion mobility, resulting in sharper peaks and higher currents compared to room temperature. However, at 100˚C, similar trends are observed, with better-defined peaks at lower current rates and broader peaks with reduced efficiency at higher currents. These observations highlight the interplay between temperature, current rate, and cycling in optimizing the electrochemical performance of LIBs.

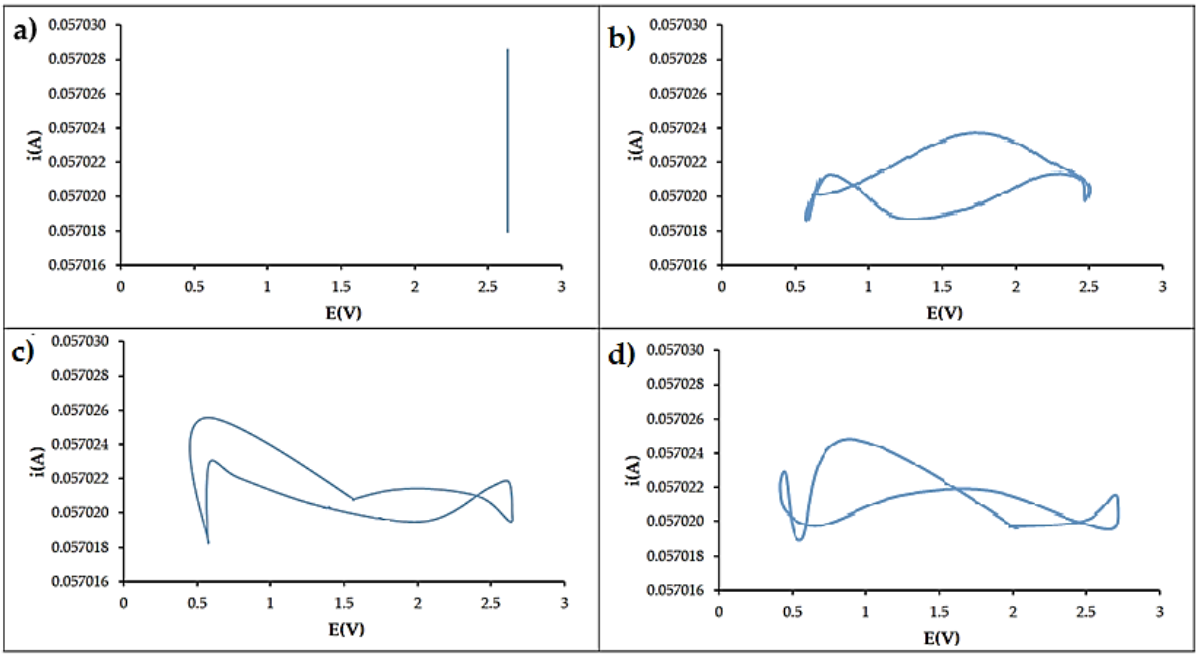

Figure 4.12 CV data at 100˚C temperature a) Fresh cell b) After 100th cycle at 100 mA current rate c) After 100th cycle at 300 mA current rate d) After 100th cycle at 500 mA current rate

4.3 OPTICAL SPECTROSCOPY ANALYSIS

The surface morphology, phase transitions, and grain structure of the anode material undergo significant transformations with increasing cycling currents, as illustrated in Figures 4.13 to 4.16. For the fresh cell, the anode surface is smooth with a uniform texture, and the grains are well-defined, indicative of pristine and uncycled material. This pristine state reflects the absence of electrochemical stress, ensuring optimal ion transport and reaction kinetics. At 100 mA, the surface begins to exhibit slight roughness, signaling the onset of electrochemical degradation. Minor phase transitions occur, accompanied by a slight blurring of grain boundaries, which suggests early-stage structural reorganization of the electrode material. These changes can be attributed to localized ion intercalation and deintercalation processes. While lithium plating is not a concern at this moderate current rate, the formation of microstructural defects can serve as precursors for future degradation. As the cycling current increases to 300 mA, surface roughness becomes more pronounced, with visible deposits and material clustering appearing on the anode. These deposits reflect uneven lithium-ion distribution and local concentration gradients, often leading to intermediate phase transitions within the anode material. The blurring of grain boundaries intensifies, and areas of localized stress become evident. At this stage, signs of uneven lithium deposition start to emerge, potentially marking the

initial stages of lithium plating in microdomains, especially under conditions of high overpotential. At 500 mA, the anode surface undergoes severe degradation, marked by heavy roughening, and irregularities. The grain boundaries, as highlighted by circles in Figures 4.13 to 4.16, exhibit significant fragmentation and irregularity. This observation underscores the effects of substantial material fatigue and mechanical stress induced by repeated cycling. The progressive deterioration of the grain structure reflects the cumulative impact of the cyclic load, contributing to the degradation of the material's integrity. Lithium plating at this stage is extensive, as high local current densities promote the deposition of metallic lithium on the surface instead of intercalation into the anode structure. This not only reduces the available active material for reversible reactions but also increases the risk of internal short circuits, compromising battery safety and performance.

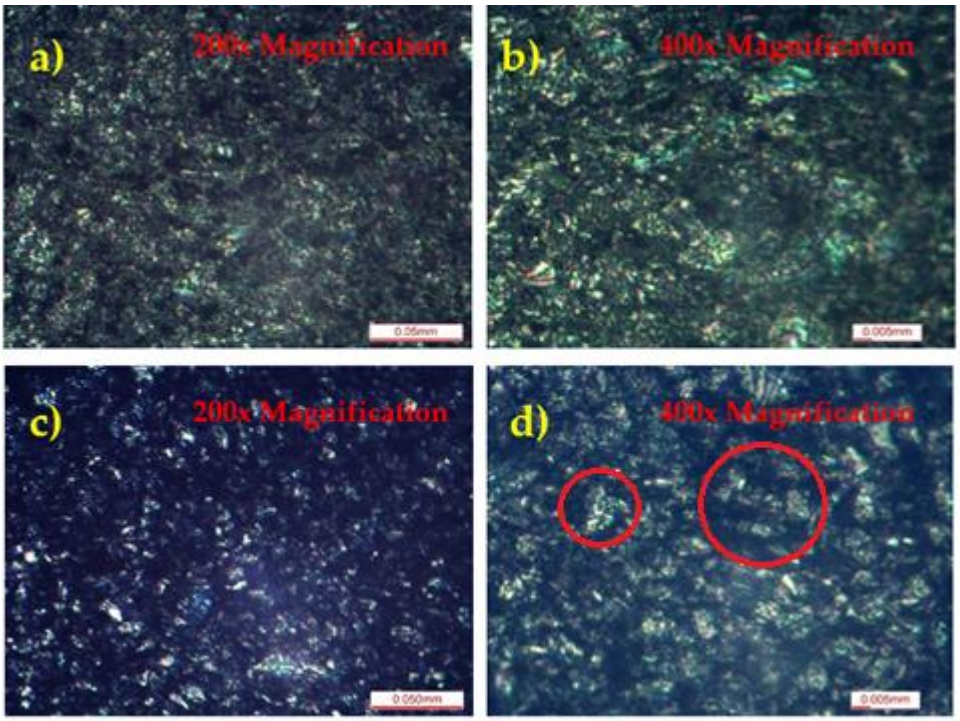

Figure 4.13 Optical spectroscopy at room temperature of a) Fresh cell (200x magnification) b) Fresh cell (400x magnification) c) Cell after cycled at 100mA constant current (200x magnification) d) Cell after cycled at 100mA constant current (400x magnification)

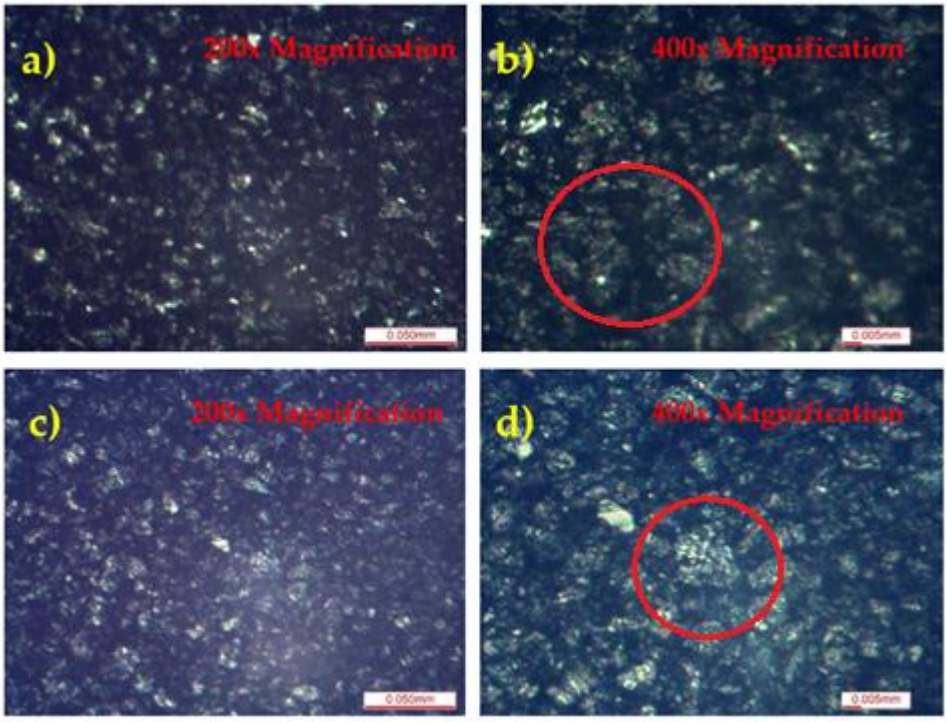

Figure 4.14 Optical spectroscopy at room temperature of a) Cell after cycled at 300mA constant current (200x magnification) b) Cell after cycled at 300mA constant current (400x magnification) c) Cell after cycled at 500mA constant current (200x magnification) d) Cell after cycled at 500mA constant current (400x magnification)

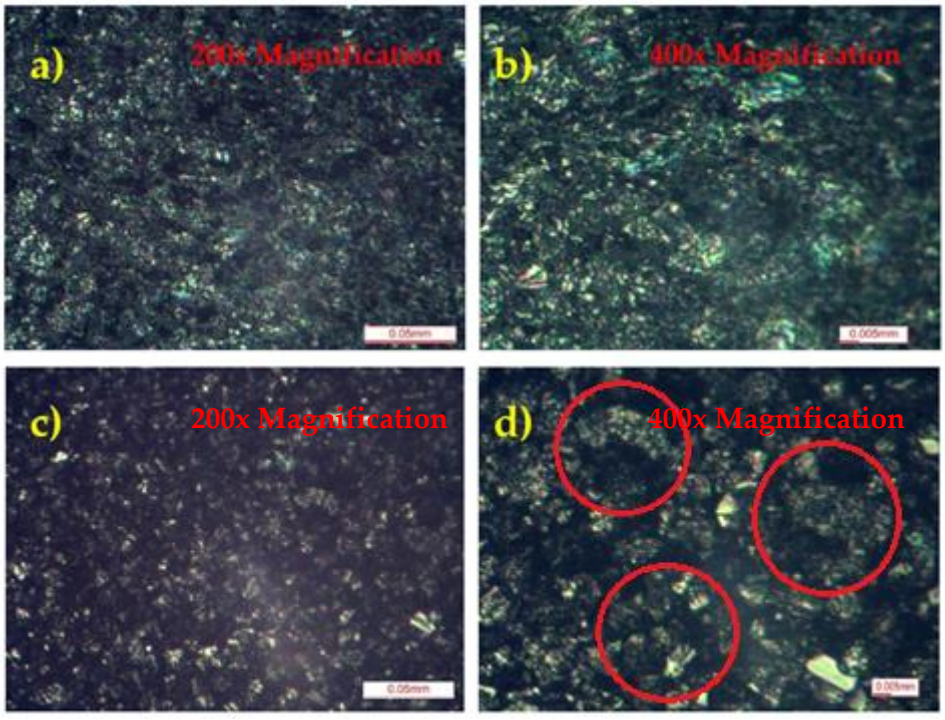

Figure 4.15 Optical spectroscopy at 100˚C temperature of a) Fresh cell (200x magnification) b) Fresh cell (400x magnification) c) Cell after cycled at 100mA constant current (200x magnification) d) Cell after cycled at 100mA constant current (400x magnification)

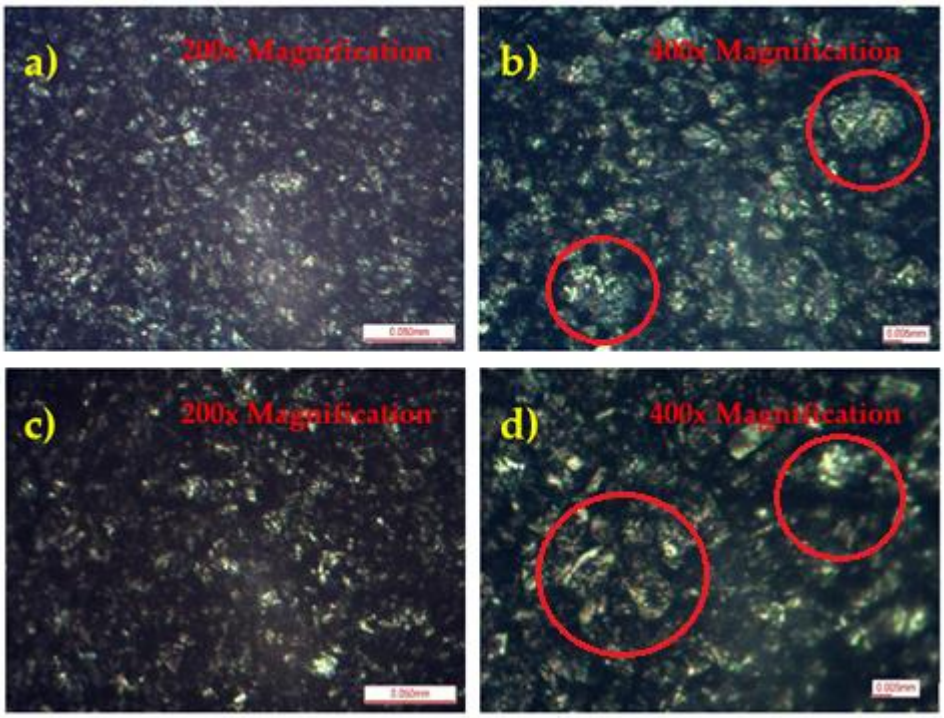

Figure 4.16 Optical spectroscopy at 100°C temperature of a) Cell after cycled at 300mA constant current (200x magnification) b) Cell after cycled at 300mA constant current (400x magnification) c) Cell after cycled at 500mA constant current (200x magnification) d) Cell after cycled at 500mA constant current (400x magnification)

Chapter 5

Conclusion and Future Study

5.1 CONCLUSIONS

In this study, a 600mAh pouch cell was tested at room temperature and 100°C to evaluate its cyclic performance, internal resistance, and structural changes after repeated charge-discharge cycles. The key findings are summarized as follows:

- Cyclic performance
  - The battery capacity decreased significantly after the first cycle, likely due to the formation of the solid electrolyte interphase (SEI) layer. Capacity also faded when the current rate and temperature was increased.
  - Coulombic efficiency was fluctuated above 100%, indicating possible side reactions.
  - Internal short circuits were observed at discharge currents of 300mA and 500mA, with abnormal behavior at 100°C and 500mA current rate.
- EIS and CV analysis
  - EIS revealed high initial impedance, attributed to incomplete SEI layer formation, suboptimal electrolyte wetting, and poor electrode interface stability. Impedance reduced for all the cases compared to fresh cell due to faster ion diffusion, reaction kinetics and transitions from a resistive-dominated to a kinetics-dominated regime.
  - CV analysis indicated anomalies inside the battery when it was cycled at elevated temperature and high current rate. Internal short circuit was responsible for not following the ideal curve of CV. As a result, too many chemical reactions were occurring during its operation.
- Optical microscopy observations
  - The anode surface exhibited severe degradation under high current rates, including roughening, and irregularities.
  - Fragmented grain boundaries and extensive lithium plating were observed, reducing active material availability and increasing the risk of internal short circuits.

5.2 LIMITATIONS

Throughout the investigation, a number of limitations have been identified. The limitations of this study are listed as follows:

- The cyclic performance test was limited to 100 cycles. Although this provides valuable insights into early-stage degradation, it may not reflect the long-term performance and failure mechanisms typically observed in lithium-ion batteries with extended cycling. This limitation was due to practical constraints, as each cycle required approximately one hour to complete, making additional cycles time-intensive.
- Optical microscopy was used to examine the anode. However, this technique is limited to surface-level observations and does not provide insights into internal structural changes. Advanced imaging techniques, such as scanning electron microscopy (SEM) or transmission electron microscopy (TEM), could offer more detailed analyses.

5.3 FUTURE STUDY

This study primarily focused on the performance of lithium-ion batteries (LIBs) at elevated operating temperatures. However, LIBs are also frequently subjected to low-temperature environments, where their performance deteriorates due to various factors, such as reduced ion mobility, slower reaction kinetics, and increased internal resistance. The behavior and mechanisms underlying these performance reductions at low temperatures remain a critical area for further exploration. Moreover, the performance and degradation characteristics of commercial LIBs operating under cryogenic conditions remain largely unexplored. Investigating the effects of extreme low temperatures on LIBs could provide valuable insights into improving their performance and reliability in applications such as aerospace, polar expeditions, and cryogenic systems. Future research should aim to address these gaps, focusing on the electrochemical, thermal, and mechanical challenges of LIBs in low-temperature and cryogenic environments.

References

[1] Alva G, Lin Y, Fang G. An overview of thermal energy storage systems. Energy 2018;144:341–78. https://doi.org/10.1016/J.ENERGY.2017.12.037.

[2] Ould Amrouche S, Rekioua D, Rekioua T, Bacha S. Overview of energy storage in renewable energy systems. Int J Hydrogen Energy 2016;41:20914–27. https://doi.org/10.1016/J.IJHYDENE.2016.06.243.

[3] Lawder MT, Suthar B, Northrop PWC, De S, Hoff CM, Leitermann O, et al. Battery energy storage system (BESS) and battery management system (BMS) for grid-scale applications. Proc IEEE 2014;102:1014–30. https://doi.org/10.1109/JPROC.2014.2317451.

[4] Yang Y, Bremner S, Menictas C, Kay M. Battery energy storage system size determination in renewable energy systems: A review. Renew Sustain Energy Rev 2018;91:109–25. https://doi.org/10.1016/J.RSER.2018.03.047.

[5] Oudalov A, Chartouni D, Ohler C. Optimizing a Battery Energy Storage System for Primary Frequency Control. IEEE Trans Power Syst 2007;22:1259–66. https://doi.org/10.1109/TPWRS.2007.901459.

[6] Belyakov N. Concept of energy. Sustain Power Gener 2019:3–22. https://doi.org/10.1016/B978-0-12-817012-0.00010-4.

[7] Vijjapu R, Tiwari S. Thermodynamics of Sensible Thermal Energy Storage Systems. Encycl Energy Storage Vol 1-4 2022;1–4:171–85. https://doi.org/10.1016/B978-0-12-819723-3.00149-9.

[8] Saleem AM, Desmaris V, Enoksson P. Performance Enhancement of Carbon Nanomaterials for Supercapacitors. J Nanomater 2016;2016:1537269. https://doi.org/10.1155/2016/1537269.

[9] SARJEANT W, ZIRNHELD J, MACDOUGALL F, BOWERS J, CLARK N, CLELLAND I, et al. Capacitors—Past, Present, and Future. Handb Low High Dielectr Constant Mater Their Appl 1999:423–91. https://doi.org/10.1016/B978-012513905-2/50023-6.

[10] Nomoto S, Nakata H, Yoshioka K, Yoshida A, Yoneda H. Advanced capacitors and their application. J Power Sources 2001;97–98:807–11. https://doi.org/10.1016/S0378-7753(01)00612-7.

[11] Béguin F, Frackowiak E. Supercapacitors: Materials, Systems, and Applications. Supercapacitors Mater Syst Appl 2013. https://doi.org/10.1002/9783527646661.

[12] Sharma S, Chand P. Supercapacitor and electrochemical techniques: A brief review. Results Chem 2023;5:100885. https://doi.org/10.1016/J.RECHEM.2023.100885.

[13] Mekhilef S, Saidur R, Safari A. Comparative study of different fuel cell technologies. Renew Sustain Energy Rev 2012;16:981–9. https://doi.org/10.1016/J.RSER.2011.09.020.

[14] Landi BJ, Ganter MJ, Cress CD, DiLeo RA, Raffaelle RP. Carbon nanotubes for lithium ion batteries. Energy Environ Sci 2009;2:638–54. https://doi.org/10.1039/B904116H.

[15] Ruetschi P. Review on the lead—acid battery science and technology. J Power Sources 1977;2:3–120. https://doi.org/10.1016/0378-7753(77)85003-9.

[16] Lopes PP, Stamenkovic VR. Past, present, and future of lead–acid batteries. Science (80-) 2020;369:923–4. https://doi.org/10.1126/SCIENCE.ABD3352.

[17] Blumbergs E, Serga V, Platacis E, Maiorov M, Shishkin A. Cadmium Recovery from Spent Ni-Cd Batteries: A Brief Review. Met 2021, Vol 11, Page 1714 2021;11:1714. https://doi.org/10.3390/MET11111714.

[18] Jeyaseelan C, Jain A, Khurana P, Kumar D, Thatai S. Ni-Cd Batteries. Recharg Batter 2020:177–94. https://doi.org/10.1002/9781119714774.CH9.

[19] Dhar SK, Ovshinsky SR, Gifford PR, Corrigan DA, Fetcenko MA, Venkatesan S. Nickel/metal hydride technology for consumer and electric vehicle batteries—a review and up-date. J Power Sources 1997;65:1–7. https://doi.org/10.1016/S0378-7753(96)02599-2.

[20] Arun V, Kannan R, Ramesh S, Vijayakumar M, Raghavendran PS, Siva Ramkumar M, et al. Review on Li-Ion Battery vs Nickel Metal Hydride Battery in EV. Adv Mater Sci Eng 2022;2022:7910072. https://doi.org/10.1155/2022/7910072.

[21] Chombo PV, Laoonual Y. A review of safety strategies of a Li-ion battery. J Power Sources 2020;478:228649. https://doi.org/10.1016/J.JPOWSOUR.2020.228649.

[22] Manthiram A. An Outlook on Lithium Ion Battery Technology. ACS Cent Sci 2017;3:1063–9. https://doi.org/10.1021/ACSCENTSCI.7B00288/ASSET/IMAGES/LARGE/OC-2017-002885_0004.JPEG.

[23] Li M, Lu J, Chen Z, Amine K. 30 Years of Lithium-Ion Batteries. Adv Mater 2018;30:1800561. https://doi.org/10.1002/ADMA.201800561.

[24] Spellman FR. The science of lithium 2024:287.

[25] Chen Y, Kang Y, Zhao Y, Wang L, Liu J, Li Y, et al. A review of lithium-ion battery safety concerns: The issues, strategies, and testing standards. J Energy Chem 2021;59:83–99. https://doi.org/10.1016/J.JECHEM.2020.10.017.

[26] An Z, Jia L, Ding Y, Dang C, Li X. A review on lithium-ion power battery thermal management technologies and thermal safety. J Therm Sci 2017;26:391–

412. https://doi.org/10.1007/s11630-017-0955-2.

[27] Zhang SS, Xu K, Jow TR. Low-temperature performance of Li-ion cells with a LiBF4-based electrolyte. J Solid State Electrochem 2003;7:147–51. https://doi.org/10.1007/s10008-002-0300-9.

[28] Jaguemont J, Boulon L, Dubé Y, Poudrier D. Low temperature discharge cycle tests for a lithium ion cell. 2014 IEEE Veh Power Propuls Conf VPPC 2014 2014. https://doi.org/10.1109/VPPC.2014.7007097.

[29] Jaguemont J, Boulon L, Dubé Y. A comprehensive review of lithium-ion batteries used in hybrid and electric vehicles at cold temperatures. Appl Energy 2016;164:99–114. https://doi.org/10.1016/J.APENERGY.2015.11.034.

[30] Keil P, Jossen A. Improving the low-temperature performance of electric vehicles by hybrid energy storage systems. 2014 IEEE Veh Power Propuls Conf VPPC 2014 2014. https://doi.org/10.1109/VPPC.2014.7007087.

[31] Zhang SS, Xu K, Jow TR. The low temperature performance of Li-ion batteries. J Power Sources 2003;115:137–40. https://doi.org/10.1016/S0378-7753(02)00618-3.

[32] Petzl M, Danzer MA. Nondestructive detection, characterization, and quantification of lithium plating in commercial lithium-ion batteries. J Power Sources 2014;254:80–7. https://doi.org/10.1016/j.jpowsour.2013.12.060.

[33] Liu H, Wei Z, He W, Zhao J. Thermal issues about Li-ion batteries and recent progress in battery thermal management systems: A review. Energy Convers Manag 2017;150:304–30. https://doi.org/10.1016/j.enconman.2017.08.016.

[34] Xiao M, Choe SY. Theoretical and experimental analysis of heat generations of a pouch type LiMn2O4/carbon high power Li-polymer battery. J Power Sources 2013;241:46–55. https://doi.org/10.1016/J.JPOWSOUR.2013.04.062.

[35] Wang Q, Ping P, Zhao X, Chu G, Sun J, Chen C. Thermal runaway caused fire and explosion of lithium ion battery. J Power Sources 2012;208:210–24. https://doi.org/10.1016/J.JPOWSOUR.2012.02.038.

[36] Wang Q, Ping P, Zhao X, Chu G, Sun J, Chen C. Thermal runaway caused fire and explosion of lithium ion battery. J Power Sources 2012;208:210–24. https://doi.org/10.1016/j.jpowsour.2012.02.038.

[37] Feng X, Fang M, He X, Ouyang M, Lu L, Wang H, et al. Thermal runaway features of large format prismatic lithium ion battery using extended volume accelerating rate calorimetry. J Power Sources 2014;255:294–301. https://doi.org/10.1016/J.JPOWSOUR.2014.01.005.

[38] Paul A, Rahman MA, Barua N. Study of temperature cycling of commercial rechargeable lithium-ion batteries. Futur Sustain 2023;1:23–31. https://doi.org/10.55670/fpll.fusus.1.1.3.

[39] Leng F, Tan CM, Pecht M. Effect of Temperature on the Aging rate of Li Ion Battery Operating above Room Temperature. Nat Publ Gr 2015:1–12. https://doi.org/10.1038/srep12967.

[40] Bodenes L, Naturel R, Martinez H, Dedryvère R, Menetrier M, Croguennec L, et al. Lithium secondary batteries working at very high temperature: Capacity fade and understanding of aging mechanisms. J Power Sources 2013;236:265–75. https://doi.org/10.1016/j.jpowsour.2013.02.067.

[41] Robinson JB, Shearing PR, Brett DJL. Thermal imaging of electrochemical power systems: A review. J Imaging 2016;2. https://doi.org/10.3390/jimaging2010002.

[42] Raijmakers LHJ, Danilov DL, Eichel RA, Notten PHL. A review on various temperature-indication methods for Li-ion batteries. Appl Energy 2019;240:918–45. https://doi.org/10.1016/j.apenergy.2019.02.078.

[43] Zhang C, Li K, Deng J. Real-time estimation of battery internal temperature based on a simplified thermoelectric model. J Power Sources 2016;302:146–54. https://doi.org/10.1016/J.JPOWSOUR.2015.10.052.

[44] Drake SJ, Martin M, Wetz DA, Ostanek JK, Miller SP, Heinzel JM, et al. Heat generation rate measurement in a Li-ion cell at large C-rates through temperature and heat flux measurements. J Power Sources 2015;285:266–73. https://doi.org/10.1016/J.JPOWSOUR.2015.03.008.

[45] Kim JH, Lee SJ, Lee JM, Cho BH. A new direct current internal resistance and state of chArge relationship for the li-ion battery pulse power estimation. 7th Internatonal Conf Power Electron ICPE'07 2007:1173–8. https://doi.org/10.1109/ICPE.2007.4692563.

[46] Schweiger HG, Obeidi O, Komesker O, Raschke A, Schiemann M, Zehner C, et al. Comparison of Several Methods for Determining the Internal Resistance of Lithium Ion Cells. Sensors 2010, Vol 10, Pages 5604-5625 2010;10:5604–25. https://doi.org/10.3390/S100605604.

[47] Kuntinugunetanon S, Meesiri W, Wongkokua W. Internal resistance measurements of Li-ion batteries using AC methods. J Phys Conf Ser 2021;1719. https://doi.org/10.1088/1742-6596/1719/1/012045.

[48] Pm VN, Ram HS, Uthan P, Veeramani V, Subramaniam S. Estimating the Internal Resistance of Li-Ion Battery with Joule's Law to find the Open Circuit Voltage. IEACon 2021 - 2021 IEEE Ind Electron Appl Conf 2021:146–50. https://doi.org/10.1109/IEACON51066.2021.9654792.

[49] Wang YW, Shu CM. Energy generation mechanisms for a Li-ion cell in case of thermal explosion: A review. J Energy Storage 2022;55:105501. https://doi.org/10.1016/J.EST.2022.105501.

[50] Saito Y, Shikano M, Kobayashi H. Heat generation behavior during charging

and discharging of lithium-ion batteries after long-time storage. J Power Sources 2013;244:294–9. https://doi.org/10.1016/J.JPOWSOUR.2012.12.124.

[51] Nazari A, Farhad S. Heat generation in lithium-ion batteries with different nominal capacities and chemistries. Appl Therm Eng 2017;125:1501–17. https://doi.org/10.1016/J.APPLTHERMALENG.2017.07.126.

[52] Kobayashi Y, Miyashiro H, Kumai K, Takei K, Iwahori T, Uchida I. Precise Electrochemical Calorimetry of LiCoO2/Graphite Lithium-Ion Cell : Understanding Thermal Behavior and Estimation of Degradation Mechanism. J Electrochem Soc 2002;149:A978. https://doi.org/10.1149/1.1487833.

[53] Zhang X, Zhang X, Sun X, An Y, Song S, Li C, et al. Electrochemical impedance spectroscopy study of lithium-ion capacitors: Modeling and capacity fading mechanism. J Power Sources 2021;488:229454. https://doi.org/10.1016/J.JPOWSOUR.2021.229454.

[54] Lee SH, Huang C, Grant PS. High energy lithium ion capacitors using hybrid cathodes comprising electrical double layer and intercalation host multi-layers. Energy Storage Mater 2020;33:408–15. https://doi.org/10.1016/J.ENSM.2020.08.022.

[55] Wu J. Understanding the Electric Double-Layer Structure, Capacitance, and Charging Dynamics. Chem Rev 2022;122:10821–59. https://doi.org/10.1021/ACS.CHEMREV.2C00097/ASSET/IMAGES/MEDIUM/CR2C00097_0029.GIF.

[56] Choi W, Shin HC, Kim JM, Choi JY, Yoon WS. Modeling and applications of electrochemical impedance spectroscopy (Eis) for lithium-ion batteries. J Electrochem Sci Technol 2020;11:1–13. https://doi.org/10.33961/JECST.2019.00528.

[57] Zhang SS, Xu K, Jow TR. EIS study on the formation of solid electrolyte interface in Li-ion battery. Electrochim Acta 2006;51:1636–40. https://doi.org/10.1016/J.ELECTACTA.2005.02.137.

[58] Liu L, Zhu M. Modeling of SEI Layer Growth and Electrochemical Impedance Spectroscopy Response using a Thermal-Electrochemical Model of Li-ion Batteries. ECS Trans 2014;61:43–61. https://doi.org/10.1149/06127.0043ECST/XML.

[59] Gourdin G, Collins J, Zheng D, Foster M, Qu D. Spectroscopic compositional analysis of electrolyte during initial SEI layer formation. J Phys Chem C 2014;118:17383–94. https://doi.org/10.1021/JP504181B/SUPPL_FILE/JP504181B_SI_001.PDF.

[60] Zhang M, Liu Y, Li D, Cui X, Wang L, Li L, et al. Electrochemical Impedance Spectroscopy: A New Chapter in the Fast and Accurate Estimation of the State of Health for Lithium-Ion Batteries. Energies 2023, Vol 16, Page 1599

2023;16:1599. https://doi.org/10.3390/EN16041599.

[61] Zhang SS, Xu K, Jow TR. Electrochemical impedance study on the low temperature of Li-ion batteries. Electrochim Acta 2004;49:1057–61. https://doi.org/10.1016/J.ELECTACTA.2003.10.016.

[62] Vadhva P, Hu J, Johnson MJ, Stocker R, Braglia M, Brett DJL, et al. Electrochemical Impedance Spectroscopy for All-Solid-State Batteries: Theory, Methods and Future Outlook. ChemElectroChem 2021;8:1930–47. https://doi.org/10.1002/CELC.202100108.

[63] Wang S, Zhang J, Gharbi O, Vivier V, Gao M, Orazem ME. Electrochemical impedance spectroscopy. Nat Rev Methods Prim 2021;1. https://doi.org/10.1038/S43586-021-00039-W.

[64] Lasia A. Electrochemical impedance spectroscopy and its applications. Electrochem Impedance Spectrosc Its Appl 2014;9781461489337:1–367. https://doi.org/10.1007/978-1-4614-8933-7/COVER.

[65] Orazem ME, Tribollet B. A tutorial on electrochemical impedance spectroscopy. ChemTexts 2020;6. https://doi.org/10.1007/S40828-020-0110-7.

[66] Hassini M, Redondo-Iglesias E, Venet P. Lithium–Ion Battery Data: From Production to Prediction. Batter 2023, Vol 9, Page 385 2023;9:385. https://doi.org/10.3390/BATTERIES9070385.

[67] Pradhan SK, Chakraborty B. Battery management strategies: An essential review for battery state of health monitoring techniques. J Energy Storage 2022;51:104427. https://doi.org/10.1016/J.EST.2022.104427.

[68] Zenati A, Desprez P, Razik H. Estimation of the SOC and the SOH of Li-ion batteries, by combining impedance measurements with the fuzzy logic inference. IECON Proc (Industrial Electron Conf 2010:1773–8. https://doi.org/10.1109/IECON.2010.5675408.

[69] Mingant R, Bernard J, Sauvant Moynot V, Delaille A, Mailley S, Hognon J-L, et al. EIS Measurements for Determining the SoC and SoH of Li-Ion Batteries. ECS Trans 2011;33:41–53. https://doi.org/10.1149/1.3589920/XML.

[70] Wang H, He L, Sun J, Liu S, Wu F. Study on correlation with SOH and EIS model of Li-ion battery. Proc 6th Int Forum Strateg Technol IFOST 2011 2011;1:261–4. https://doi.org/10.1109/IFOST.2011.6021018.

[71] Liu Y, Wang L, Li D, Wang K. State-of-health estimation of lithium-ion batteries based on electrochemical impedance spectroscopy: a review. Prot Control Mod Power Syst 2023;8:1–17. https://doi.org/10.1186/S41601-023-00314-W/TABLES/6.

[72] Li Y, Li K, Liu X, Li X, Zhang L, Rente B, et al. A hybrid machine learning framework for joint SOC and SOH estimation of lithium-ion batteries assisted

with fiber sensor measurements. Appl Energy 2022;325:119787. https://doi.org/10.1016/J.APENERGY.2022.119787.

[73] Akbar K, Zou Y, Awais Q, Baig MJA, Jamil M. A Machine Learning-Based Robust State of Health (SOH) Prediction Model for Electric Vehicle Batteries. Electron 2022, Vol 11, Page 1216 2022;11:1216. https://doi.org/10.3390/ELECTRONICS11081216.

[74] Tao T, Ji C, Dai J, Rao J, Wang J, Sun W, et al. Data-based health indicator extraction for battery SOH estimation via deep learning. J Energy Storage 2024;78:109982. https://doi.org/10.1016/J.EST.2023.109982.

[75] Braĭnina KZ., Neyman E. Electroanalytical stripping methods 1993:198.

[76] Lindström H, Södergren S, Solbrand A, Rensmo H, Hjelm J, Hagfeldt A, et al. Li+ Ion Insertion in TiO2 (Anatase). 1. Chronoamperometry on CVD Films and Nanoporous Films. J Phys Chem B 1997;101:7710–6. https://doi.org/10.1021/JP970489R.

[77] Chesney DJ. Laboratory Techniques in Electroanalytical Chemistry, 2nd Edition Edited by Peter T. Kissinger (Purdue University) and William R. Heineman (University of Cincinnati). Dekker: Monticello, NY. 1996. xxii + 986 pp. $79. ISBN 0-8247-9445-1. J Am Chem Soc 1996;118:10946–10946. https://doi.org/10.1021/JA965572R.

[78] Kim T, Choi W, Shin HC, Choi JY, Kim JM, Park MS, et al. Applications of Voltammetry in Lithium Ion Battery Research. J Electrochem Sci Technol 2020;11:14–25. https://doi.org/10.33961/JECST.2019.00619.

[79] Bard AJ, Faulkner LR. Polarography and Pulse Voltammetry. Electrochem Methods Fundam Appl 2001:261–304.

[80] Siclovan OP, Zappi G, Soloveichik GL. High-temperature cyclic voltammetry in non-aqueous solvents. ECS Electrochem Lett 2014;3:H41–3. https://doi.org/10.1149/2.0051412EEL/XML.

[81] Lindström H, Södergren S, Solbrand A, Rensmo H, Hjelm J, Hagfeldt A, et al. Li+ ion insertion in TiO2 (anatase) .2. Voltammetry on nanoporous films. J Phys Chem B 1997;101:7717–22.

[82] Amemiya S. Scanning Electrochemical Microscopy. Charact Mater 2012:1–13. https://doi.org/10.1002/0471266965.COM053.PUB2.

[83] Guidelli R, Compton RG, Feliu JM, Gileadi E, Lipkowski J, Schmickler W, et al. Defining the transfer coefficient in electrochemistry: An assessment (IUPAC Technical Report). Pure Appl Chem 2014;86:245–58. https://doi.org/10.1515/PAC-2014-5026/MACHINEREADABLECITATION/RIS.

[84] Oldham KB., Myland JC., Bond AM. Electrochemical science and technology : fundamentals and applications 2012:405.

[85] Delahay P, Tobias CW, Lander JJ. Advances in Electrochemistry and Electrochemical Engineering. J Electrochem Soc 1964;111:33C. https://doi.org/10.1149/1.2426104.

[86] Wang H, Pilon L. Physical interpretation of cyclic voltammetry for measuring electric double layer capacitances. Electrochim Acta 2012;64:130–9. https://doi.org/10.1016/J.ELECTACTA.2011.12.118.

[87] Uhlmann C, Illig J, Ender M, Schuster R, Ivers-Tiffée E. In situ detection of lithium metal plating on graphite in experimental cells. J Power Sources 2015;279:428–38. https://doi.org/10.1016/J.JPOWSOUR.2015.01.046.

[88] Aurbach D, Zinigrad E, Cohen Y, Teller H. A short review of failure mechanisms of lithium metal and lithiated graphite anodes in liquid electrolyte solutions. Solid State Ionics 2002;148:405–16. https://doi.org/10.1016/S0167-2738(02)00080-2.

[89] Aurbach D, Zinigrad E, Teller H, Dan P. Factors Which Limit the Cycle Life of Rechargeable Lithium (Metal) Batteries. J Electrochem Soc 2000;147:1274. https://doi.org/10.1149/1.1393349/XML.

[90] Ren D, Feng X, Lu L, Ouyang M, Zheng S, Li J, et al. An electrochemical-thermal coupled overcharge-to-thermal-runaway model for lithium ion battery. J Power Sources 2017;364:328–40. https://doi.org/10.1016/J.JPOWSOUR.2017.08.035.

[91] Waldmann T, Wilka M, Kasper M, Fleischhammer M, Wohlfahrt-Mehrens M. Temperature dependent ageing mechanisms in Lithium-ion batteries – A Post-Mortem study. J Power Sources 2014;262:129–35. https://doi.org/10.1016/J.JPOWSOUR.2014.03.112.

[92] Cheng XB, Zhang R, Zhao CZ, Wei F, Zhang JG, Zhang Q. A Review of Solid Electrolyte Interphases on Lithium Metal Anode. Adv Sci 2016;3:1500213. https://doi.org/10.1002/ADVS.201500213.

[93] Rosso M, Brissot C, Teyssot A, Dollé M, Sannier L, Tarascon JM, et al. Dendrite short-circuit and fuse effect on Li/polymer/Li cells. Electrochim Acta 2006;51:5334–40. https://doi.org/10.1016/J.ELECTACTA.2006.02.004.

[94] Burns JC, Dahn J. The Effect of High Charge Rate Cycling on Coulombic Efficiency Measurements. ECS Meet Abstr 2014;MA2014-02:347–347. https://doi.org/10.1149/MA2014-02/5/347.

[95] Li YC, Duh YS, Hsu JM, Kao CS. Thermal instability of organic esters and ethers with deposited lithium in lithium-ion battery. J Therm Anal Calorim 2014;116:1219–26. https://doi.org/10.1007/S10973-014-3689-3.

[96] Yuan QF, Zhao F, Wang W, Zhao Y, Liang Z, Yan D. Overcharge failure investigation of lithium-ion batteries. Electrochim Acta 2015;C:682–8. https://doi.org/10.1016/J.ELECTACTA.2015.07.147.

[97] Crowther O, West AC. Effect of Electrolyte Composition on Lithium Dendrite Growth. J Electrochem Soc 2008;155:A806. https://doi.org/10.1149/1.2969424/XML.

[98] Steiger J, Kramer D, Mönig R, Steiger J, Kramer D, Mönig R. Mechanisms of dendritic growth investigated by in situ light microscopy during electrodeposition and dissolution of lithium. JPS 2014;261:112–9. https://doi.org/10.1016/J.JPOWSOUR.2014.03.029.

[99] Nishikawa K, Mori T, Nishida T, Fukunaka Y, Rosso M, Homma T. In situ observation of dendrite growth of electrodeposited Li metal. J Electrochem Soc 2010;157:A1212–7. https://doi.org/10.1149/1.3486468.

[100] Guo Z, Zhu J, Feng J, Du S. Direct in situ observation and explanation of lithium dendrite of commercial graphite electrodes. RSC Adv 2015;5:69514–21. https://doi.org/10.1039/C5RA13289D.

[101] Systems BT. Battery Test Systems V7.0 Software Instruction Manual 2019.

[102] Sun J, Chen S, Xing S, Guo Y, Wang S, Wang R, et al. A battery internal short circuit fault diagnosis method based on incremental capacity curves. J Power Sources 2024;602:234381. https://doi.org/10.1016/J.JPOWSOUR.2024.234381.

Appendix-I
Data

I. INTRODUCTION

Data were collected from the experimental setup and graphical representation was made by those data.

I.I DATA FILTRATION AND ANALYSIS

Figure I.I illustrates the data analysis and filtration process employed in the study. The analysis was conducted using Microsoft Excel, which facilitated the organization, processing, and visualization of the experimental data. The software was instrumental in performing calculations, generating plots, and ensuring accurate interpretation of the results.

Figure I.I Data filtration method

I.II EXPERIMENTAL DATA

The experimental data are presented in tables, comparing the performance of different battery cells under varying conditions. These include measurements taken at room temperature and at 100°C, across a range of current rates.

I.II.I Data Collected at Room Temperature

All the table shows the capacity of the battery during charging and discharging at 28°C (Room Temperature) when the battery was cycled at 100mA, 300mA, and 500mA constant current.

I.II.I.I Constant Current 100mA

Table I.I shows charging capacity, discharging capacity and coulombic efficiency of the battery when the current rate was 100mA.

Table I.I Performance data of battery at 100mA constant current

Cycle	CapC/mAh	CapD/mAh	Efficiency/%
1	0	58.1	0
2	9.2	9.6	104.23
3	9.3	9.5	101.79
4	8.9	9	100.93
5	8.7	8.8	100.96
6	8.8	8.8	100.63
7	7.1	8.9	125.98
8	8.8	8.9	101.58
9	10.6	10.6	100.53
10	11.1	11.3	101.25
11	11.4	11.4	100
12	11.5	10	87.41
13	9.6	9.6	99.14
14	9.1	9.1	100
15	8.6	8.6	100
16	8.5	8.5	100
17	8.1	8.2	100.34
18	8	8.1	100.69
19	9.8	9.8	100
20	8.7	8.8	100.32
21	8.5	8.6	100.65

Cycle	CapC/mAh	CapD/mAh	Efficiency/%
22	10.2	10.3	100.54
23	11	9.6	86.9
24	11.7	11.8	100.24
25	11.8	11.8	100.24
26	11.8	11.8	100.24
27	11.9	11.9	100.47
28	12	12	100
29	12	12	100.23
30	11.9	11.9	100.23
31	11.9	12	100.47
32	10.8	11.7	107.97
33	12	12	100.23
34	12.1	11.8	97.93
35	12	12	100
36	10.5	10.5	100.27
37	9.8	9.8	100.28
38	9.1	9.2	100.91
39	9.1	9.1	100.31
40	8.8	8.8	100.64
41	8.4	8.5	100.99
42	10.6	10.6	100
43	11.1	11.1	100.25
44	11.3	11.3	100.25
45	11.5	11.5	99.76
46	9.5	9.6	100.88
47	10.9	11	100.76
48	11.4	11.4	100.24
49	11.6	11.6	100.24
50	11.7	11.7	100
51	11.8	11.8	100.24
52	11.9	11.9	100.23
53	11.9	12	100.23
54	12	12	100
55	12	12	100.46
56	12.1	12.1	100.23
57	11	11	100
58	9.7	9.8	100.29
59	9.6	9.7	100.87
60	11.3	11.3	100
61	11.7	11.8	100.24
62	11.8	11.9	100.23

Cycle	CapC/mAh	CapD/mAh	Efficiency/%
63	11.9	11.9	100
64	11.5	12	104.84
65	12.1	11.5	95.62
66	12.1	12	99.08
67	12.1	12.2	100.23
68	12.2	11.4	94.06
69	11.2	11.4	101.99
70	12	12	100
71	11.6	11.6	99.52
72	10.1	10.1	100.55
73	9.6	9.7	100.58
74	9.4	9.4	100
75	9	6.7	74.07
76	9.2	9.2	100.3
77	9.1	9.1	100
78	8.8	8.8	100.32
79	10.3	10.4	100.54
80	11	11	100.25
81	11.3	11.3	100.25
82	11.5	11.5	100
83	11.6	11.6	100.48
84	11.7	11.8	100.71
85	11.8	11.8	100.24
86	11.8	11.6	98.35
87	10.5	10.5	100.27
88	9.5	9.5	100.29
89	10.7	10.8	100.78
90	11.3	11.4	100.49
91	11.5	11.6	100.24
92	11.7	11.7	100.24
93	11.9	11.9	100.23
94	12	12	100.23
95	12	12	100
96	12.1	12.1	100
97	12.1	12.1	100.23
98	12.1	12.2	100.46
99	12.2	12.2	100.23
100	12.2	0	0

I.II.I.II Constant Current 300mA

Table I.II shows charging capacity, discharging capacity and coulombic efficiency of the battery when the current rate was 300mA.

Table I.II Performance data of battery at 300mA constant current

Cycle	CapC/mAh	CapD/mAh	Efficiency/%
1	0.2	58.3	0
2	4.7	5.8	122.81
3	4.3	4.9	113.46
4	4.1	4.5	110.21
5	3.8	4.1	106.52
6	3.7	4	106.66
7	3.7	3.8	104.54
8	3.6	3.7	104.65
9	3.5	3.7	107.14
10	3.5	3.7	104.76
11	3.5	3.7	104.76
12	3.5	3.7	104.76
13	3.4	3.5	102.44
14	3.4	3.6	104.88
15	3.4	3.6	104.88
16	3.5	3.7	104.76
17	3.7	3.7	102.27
18	3.7	3.1	84.09
19	3.7	3.9	106.82
20	3.7	3.8	104.55
21	3.6	3.7	104.65
22	2.8	3.2	111.76
23	3.2	3.3	102.57
24	3.2	3.4	105.13
25	3.3	3.4	102.5
26	3.3	3.5	105
27	3.6	3.7	102.32
28	3.7	3.8	104.55
29	3.8	4	104.35
30	4	4.1	102.08
31	4.1	4.2	104.08
32	4.2	4.3	104
33	4.2	4.3	101.96
34	4.2	4.2	100
35	4.2	4.4	103.92

Cycle	CapC/mAh	CapD/mAh	Efficiency/%
36	4.4	4.5	101.89
37	4.5	4.6	101.85
38	4.5	4.7	103.7
39	4.6	4.7	103.64
40	4.7	4.7	101.79
41	4.7	4.8	103.57
42	4.7	4.8	101.76
43	4.7	4.8	101.75
44	4.7	4.9	103.51
45	4.7	4.9	103.51
46	4.8	4.9	101.72
47	4.8	4.9	101.72
48	2.2	6.7	296.3
49	4.2	4.5	105.88
50	4.2	4.4	103.92
51	4.1	4.2	104.08
52	4	4.1	102.08
53	4	4.2	104.17
54	4	4.1	102.09
55	3.9	4	102.13
56	3.7	3.9	104.44
57	3.7	3.8	102.22
58	3.7	3.8	102.22
59	3.7	3.7	102.27
60	3.7	3.7	102.27
61	3.6	3.6	100
62	3.5	3.6	102.38
63	3.5	3.6	102.38
64	3.5	3.7	104.76
65	3.4	3.6	104.88
66	3.4	3.5	102.44
67	3.4	3.5	102.44
68	3.4	3.5	102.44
69	3.3	3.4	102.5
70	3.3	3.4	102.5
71	3.2	3.4	105.13
72	3.2	3.3	102.56
73	3.2	3.3	102.56
74	3.2	3.3	102.57
75	3.4	3.5	102.43
76	3.7	3.7	100

Cycle	CapC/mAh	CapD/mAh	Efficiency/%
77	3.7	3.8	102.22
78	3.8	3.9	102.18
79	3.8	3.9	102.18
80	3.7	3.9	104.44
81	3.7	3.8	104.54
82	3.6	3.7	102.33
83	3.6	3.7	102.32
84	3.6	3.7	102.32
85	3.5	3.7	104.76
86	3.5	3.7	104.76
87	3.5	3.6	102.38
88	3.7	3.7	102.27
89	3.8	3.8	100
90	3.8	3.9	102.18
91	4.1	4.2	102.04
92	4.1	4.2	104.09
93	4.2	4.3	101.96
94	4.2	4.4	103.92
95	4.4	4.5	101.88
96	4.5	4.6	101.85
97	3.2	7.7	235.88
98	4.8	5	103.45
99	4.9	5	101.7
100	5	5.2	103.33

I.II.I.III Constant Current 500mA

Table I.III shows charging capacity, discharging capacity and coulombic efficiency of the battery when the current rate was 300mA.

Table I.III Performance data of battery at 500mA constant current

Cycle	CapC/mAh	CapD/mAh	Efficiency/%
1	0.4	122.2	0
2	4.3	6.9	161.29
3	4.4	5.3	118.75
4	4	4.4	110.34
5	3.6	4	111.54
6	3.6	3.7	103.85
7	3.5	3.7	108
8	3.5	3.7	108
9	3.6	3.7	103.85
10	3.5	3.7	108
11	3.5	3.7	108
12	3.5	3.7	108
13	3.6	3.7	103.85
14	3.6	3.9	107.69
15	3.6	3.9	107.69
16	3.7	4	107.41
17	3.7	4	107.41
18	3.9	3.9	100
19	3.9	4	103.57
20	4	4.2	103.44
21	4	4.2	103.45
22	4	4.4	110.34
23	4	4.2	103.44
24	4	4.2	103.45
25	4	4.3	106.89
26	4	4.3	106.9
27	4.2	4.3	103.33
28	4.2	4.2	100
29	4	4.2	103.45
30	4	4.2	103.45
31	4.2	4.3	103.33
32	4	4.3	106.9
33	4.2	4.3	103.33
34	4.2	4.3	103.34

Cycle	CapC/mAh	CapD/mAh	Efficiency/%
35	4.2	4.3	103.33
36	4.2	4.3	103.33
37	4.2	4.3	103.33
38	4.2	4.3	103.33
39	4.3	4.4	103.23
40	4.3	4.4	103.23
41	4.2	4.3	103.34
42	4.3	4.4	103.22
43	4.3	4.4	103.22
44	4.3	4.4	103.22
45	4.3	4.4	103.23
46	4.3	4.6	106.45
47	4.3	4.4	103.23
48	4.3	4.4	103.23
49	4.3	4.4	103.22
50	4.3	4.4	103.23
51	4.3	4.4	103.22
52	4.4	4.6	103.13
53	4.3	4.4	103.22
54	4.3	4.4	103.22
55	4.3	4.4	103.23
56	4.3	4.4	103.23
57	4.4	4.6	103.13
58	4.3	4.4	103.23
59	4.2	4.3	103.33
60	4.2	4.2	100
61	4	4.2	103.45
62	4	4.2	103.45
63	4	4	100
64	3.9	4	103.57
65	4	4.2	103.45
66	3.9	4	103.57
67	4	4.2	103.45
68	4	4	100
69	4	4.2	103.45
70	4	4.2	103.44
71	4	4	100
72	4	4.2	103.45
73	4	4.2	103.45
74	4	4.2	103.44
75	4.2	4.3	103.33

Cycle	CapC/mAh	CapD/mAh	Efficiency/%
76	1.2	4	322.22
77	3.5	3.7	108
78	3.6	3.9	107.69
79	3.7	3.9	103.7
80	3.7	4	107.41
81	3.9	3.9	100
82	3.9	4	103.57
83	3.7	4	107.41
84	3.9	4	103.57
85	3.7	4	107.41
86	3.9	4	103.57
87	4	4	100
88	3.9	4	103.57
89	4	4.2	103.45
90	4	4	100
91	4	4.2	103.45
92	4	4.2	103.45
93	3.9	4	103.57
94	3.9	4	103.57
95	4	4	100
96	4	4.3	106.9
97	4.2	4.3	103.33
98	4.2	4.4	106.67
99	4.2	4.3	103.33
100	4.2	4.4	106.67

I.II.II Data Collected at 100˚C

I.II.II.I Constant Current 100mA

Table I.IV shows charging capacity, discharging capacity and coulombic efficiency of the battery when the current rate was 100mA.

Table I.IV Performance data of battery at 100mA constant current and 100˚C temperature

Cycle	CapC/mAh	CapD/mAh	Efficiency/%
1	0	226.3	0
2	9.4	10.5	111.5
3	13.7	15.2	111.18
4	15.9	17.4	109.98
5	14.4	14.5	100.58
6	15.3	15.5	101.64
7	13.4	13.3	98.84
8	13.6	14.2	104.5
9	15.6	15.6	100.53
10	13.9	13.5	96.81
11	10.8	10.9	100.78
12	11.9	12.6	105.36
13	15.8	15.9	100.35
14	14.9	14.9	99.63
15	15.9	16.2	101.75
16	15.1	15.1	99.82
17	15.8	15.6	98.77
18	15.4	15.6	101.08
19	13.8	13.4	96.98
20	12.6	13	103.31
21	15.4	15.4	99.62
22	13.6	13.5	99.39
23	14.5	14.8	102.1
24	15.3	15.1	98.19
25	13.8	13.8	100.4
26	15.4	15.7	101.98
27	14.2	14.2	100
28	14.4	12.9	89.4
29	13.6	14.3	105.53
30	16.4	16.4	99.83
31	7.1	6.6	93
32	10.5	11.4	108.73

Cycle	CapC/mAh	CapD/mAh	Efficiency/%
33	15	15.2	101.1
34	13.5	13.3	97.95
35	13.2	13.5	102.11
36	14.1	14.1	99.81
37	14.8	14.9	100.93
38	14.8	14.4	97
39	12.4	12.6	101.79
40	14.7	14.9	101.52
41	15.1	15	99.27
42	14.3	12.7	88.36
43	13	13.6	104.7
44	15.8	16	101.42
45	16.8	16.1	95.69
46	12	12	100.46
47	12.8	13.3	103.9
48	16	16.2	101.22
49	17.5	17.3	98.73
50	15.7	14.9	94.87
51	11.6	11.4	98.8
52	10.3	10.5	102.43
53	13.3	13.7	103.56
54	16.6	16.5	99.5
55	14.9	14.5	97.02
56	14.4	14.8	102.31
57	14.9	14.5	97.21
58	13.2	13.2	100
59	15	14.4	96.11
60	13.1	12.7	97.24
61	15.4	14.8	96.03
62	12.9	12.6	97.42
63	11.2	11.3	101.5
64	13.6	14	102.44
65	15.2	14.6	95.8
66	12.9	13.1	101.29
67	13.3	12.9	97.48
68	11	14.5	131.23
69	13.3	13.1	98.75
70	13.9	14	100.81
71	12.6	12.8	101.1
72	15	14.8	98.88
73	13	12.7	97.23

Cycle	CapC/mAh	CapD/mAh	Efficiency/%
74	10.8	10.9	101.29
75	12.8	13.1	102.38
76	14.6	14.1	96.76
77	11.9	12.1	101.4
78	13.7	13.5	98.78
79	11.7	11.6	99.05
80	12.4	12.8	102.9
81	14.1	13.8	97.45
82	11.6	11.4	98.54
83	11.4	11.8	102.97
84	13.6	13.6	100
85	12.5	12.6	100.66
86	6.7	7.1	106.64
87	11.4	11.6	101.22
88	13.4	13.2	98.14
89	13	12.9	99.36
90	12.5	12.4	99.33
91	13.4	13.5	100.41
92	14.1	13.7	97.24
93	11.1	11	98.75
94	10.6	10.8	102.11
95	12.5	12.6	100.67
96	12.7	12.8	100.21
97	14	13.8	98.51
98	11.7	11.6	99.29
99	12.3	12.5	101.8
100	12.9	0	0

I.II.II.II Constant Current 300mA

Table I.V shows charging capacity, discharging capacity and coulombic efficiency of the battery when the current rate was 300mA.

Table I.V Performance data of battery at 300mA constant current and 100°C temperature

Cycle	CapC/mAh	CapD/mAh	Efficiency/%
1	0	2.9	0
2	2.2	2.9	129.63
3	3.7	4.2	113.63
4	4.8	5.1	105.17
5	4.5	4.7	105.56
6	4.4	4.6	103.77
7	4.2	4.3	101.96
8	3.9	4	102.13
9	2.7	2.8	106.25
10	2.9	3.1	105.71
11	3.6	3.7	104.65
12	2.8	2.9	102.94
13	4.1	4.2	104.08
14	2.8	3.1	108.82
15	5.2	5.3	103.23
16	5.5	5.7	103.03
17	5.2	5.3	103.23
18	6	6	100
19	5.6	5.7	101.49
20	5.2	5.3	101.59
21	5.2	5.4	103.17
22	4.7	4.9	103.51
23	4.7	4.7	101.79
24	4.9	5.1	103.39
25	5.2	5.4	103.17
26	5.7	5.7	101.47
27	5.7	5.7	101.47
28	4.8	4.9	101.72
29	3.4	3.7	107.32
30	4.5	4.7	105.56
31	4.2	4.3	101.96
32	4.2	4.4	103.92
33	4.1	4.2	102.04

Cycle	CapC/mAh	CapD/mAh	Efficiency/%
34	4.1	4.2	104.08
35	3.7	3.8	102.22
36	3.9	3.9	100
37	3.6	3.7	102.33
38	3.1	3.2	102.7
39	2.9	3	102.86
40	2.7	2.8	103.03
41	2.5	2.6	103.33
42	2.3	2.4	103.57
43	2.2	2.3	107.69
44	2.1	2.2	104
45	1.9	2.1	108.7
46	1.8	2	109.09
47	2	2	100
48	1.9	2.1	108.7
49	2.1	2.2	104
50	1	1.1	108.33
51	1	1.2	125
52	1.2	1.3	114.29
53	3.2	3.2	100
54	4.1	4.2	102.04
55	4.2	4.3	104
56	4.4	4.5	101.89
57	3.9	4	102.13
58	3.7	3.8	104.55
59	3.7	3.7	102.27
60	3.5	3.6	102.38
61	4	4.1	102.08
62	3.4	3.6	104.88
63	3.2	3.2	102.63
64	4.1	4.2	102.04
65	3.5	3.6	102.38
66	3.7	3.7	102.27
67	3.5	3.7	104.76
68	4	4.1	102.08
69	3.8	3.9	102.17
70	4.1	4.2	102.04
71	3.7	3.9	104.44
72	3.7	3.9	104.45
73	4.2	4.2	100
74	4	4.2	104.16

Cycle	CapC/mAh	CapD/mAh	Efficiency/%
75	3.7	3.8	102.22
76	4	4	100
77	3.9	4	102.13
78	3.7	3.7	100
79	3.4	3.5	102.43
80	3.7	3.8	104.54
81	3.6	3.7	102.33
82	2.9	2.9	100
83	3.7	3.8	102.23
84	3.8	3.9	102.18
85	3.7	3.8	102.22
86	2.4	2.5	103.45
87	2.3	2.4	103.57
88	2.4	2.6	106.89
89	2.2	2.3	103.7
90	2.3	2.4	103.57
91	2.7	2.7	103.13
92	3	3.2	105.56
93	3.5	3.5	100
94	2.9	3	102.86
95	3.2	3.3	102.57
96	3.2	3.2	102.64
97	3.3	3.3	100
98	3.4	3.5	102.44
99	3.2	3.3	102.56
100	3.3	0	0

I.II.II.III Constant Current 500mA

Table I.VI shows charging capacity, discharging capacity and coulombic efficiency of the battery when the current rate was 500mA.

Table I.VI Performance data of battery at 500mA constant current and 100°C temperature

Cycle	CapC/mAh	CapD/mAh	Efficiency/%
1	0	3.2	0
2	3.3	3.6	108.33
3	4.9	5	102.86
4	3.3	3.6	108.33
5	4.2	4.3	103.33
6	3.1	3.2	104.54
7	3.3	3.5	104.17
8	2.9	3.2	109.53
9	2.9	3.2	109.52
10	2.8	2.9	105
11	2.9	3.2	109.53
12	3.3	3.6	108.33
13	3.5	3.6	104
14	3.6	3.8	103.84
15	2.1	2.4	113.33
16	1.3	1.5	122.21
17	1.9	2.1	107.14
18	2.1	2.2	106.66
19	2.1	2.2	106.66
20	2.2	2.4	106.25
21	1.8	2.2	123.07
22	2.2	2.4	106.25
23	2.1	2.2	106.67
24	1.9	2.1	107.14
25	1.2	1.5	122.22
26	1.4	1.4	100
27	1.1	1.2	112.5
28	1.8	1.9	107.69
29	2.4	2.5	105.89
30	1.9	2.1	107.14
31	2.8	2.8	100
32	2.1	2.4	113.34
33	2.5	2.5	100

Cycle	CapC/mAh	CapD/mAh	Efficiency/%
34	2.1	2.2	106.66
35	1.8	1.9	107.69
36	1.5	1.8	118.18
37	2.2	2.4	106.24
38	1.5	1.7	109.09
39	2.4	2.5	105.88
40	1.9	2.1	107.14
41	1.8	1.8	100
42	1.5	1.7	109.09
43	1.5	1.8	118.18
44	1.2	1.5	122.22
45	1.4	1.5	110
46	1.1	1.4	125
47	1.4	1.5	110
48	1.2	1.5	122.22
49	1.5	1.7	109.09
50	1.4	1.4	100
51	0.6	0.8	150
52	0.8	1	116.67
53	0.8	1.1	133.33
54	1.1	1.2	112.5
55	1.2	1.5	122.24
56	1.3	1.3	100.01
57	1.5	1.7	109.09
58	1.1	1.4	124.99
59	1.3	1.5	122.22
60	1	1.1	114.29
61	1.1	1.3	112.5
62	1.3	1.2	99.99
63	1.1	1.4	125.01
64	1.3	1.2	99.99
65	1.4	1.4	100.01
66	1.5	1.7	109.09
67	1.5	1.8	118.18
68	1.7	1.7	100
69	1.9	2.1	107.15
70	1.9	2.2	114.29
71	1.8	1.9	107.69
72	1.7	1.9	116.67
73	1.7	1.8	108.33
74	1.8	2.1	115.38

Cycle	CapC/mAh	CapD/mAh	Efficiency/%
75	1.9	2.1	107.14
76	1.8	1.9	107.69
77	1.8	1.9	107.69
78	1.9	2.1	107.14
79	1.8	1.8	100
80	1.7	1.8	108.33
81	1.8	1.9	107.69
82	2.1	2.2	106.67
83	1.8	1.9	107.69
84	1.9	2.1	107.14
85	1.7	1.9	116.66
86	1.5	1.7	109.09
87	2.1	2.1	100
88	2.1	2.1	100
89	1.7	1.7	100
90	1.5	1.7	109.09
91	2.1	2.2	106.67
92	1.5	1.7	109.09
93	1.4	1.5	110
94	1.5	1.7	109.09
95	1.2	1.5	122.22
96	1.2	1.5	122.22
97	1.8	1.9	107.69
98	1.9	2.1	107.14
99	1.9	2.1	107.14
100	1.9	2.1	107.14

Appendix-II

plag_check_aoyon

ORIGINALITY REPORT

17%	12%	13%	%
SIMILARITY INDEX	INTERNET SOURCES	PUBLICATIONS	STUDENT PAPERS

PRIMARY SOURCES

1	Qianqian Liu, Chunyu Du, Bin Shen, Pengjian Zuo, Xinqun Cheng, Yulin Ma, Geping Yin, Yunzhi Gao. "Understanding undesirable anode lithium plating issues in lithium-ion batteries", RSC Advances, 2016 Publication	2%
2	www.mdpi.com Internet Source	1%
3	www.ncbi.nlm.nih.gov Internet Source	1%
4	www.jecst.org Internet Source	<1%
5	lib.buet.ac.bd:8080 Internet Source	<1%
6	mdpi-res.com Internet Source	<1%
7	www.coursehero.com Internet Source	<1%
8	dspace.mist.ac.bd:8080 Internet Source	

Appendix-III

Future Sustainability
Open Access Journal
ISSN 2995-0473

November 2023| Volume 01 | Issue 01 | Pages 23-31

Journal homepage: https://fupubco.com/fusus

https://doi.org/10.55670/fpll.fusus.1.1.3

Future Publishing LLC

Article

Study of temperature cycling of commercial rechargeable lithium-ion batteries

Aoyon Paul, Md. Arafat Rahman*, Nirjhor Barua

Department of Mechanical Engineering, Chittagong University of Engineering and Technology, Chittagong-4349, Bangladesh

ARTICLE INFO

Article history:
Received 02 September 2023
Received in revised form
03 October 2023
Accepted 09 October 2023

Keywords:
Battery cycling, Capacity fade,
Temperature effects, Lithium-ion battery

*Corresponding author
Email address:
arafat@cuet.ac.bd

DOI: 10.55670/fpll.fusus.1.1.3

ABSTRACT

Lithium-ion batteries, a popular electric energy storage device, have high energy density and impressive working performance. However, the temperature affects its life cycle, capacity, and performance. Different effects are generated inside the battery for the different temperature conditions. It is necessary to study their thermal and electric characteristics in various thermal conditions since electric energy storage devices are used in various applications at low or high temperatures. In this study, the experimental analysis was performed to observe how a battery cell behaves above room temperature for a different 18650 cylindrical battery cell with a capacity of 5200 mAh. The testing temperature for this experiment was at 28°C, 50°C, 60°C, 70°C, and 100°C. It is noted that the capacity of the battery cell fades drastically at high temperatures compared to low temperatures due to internal short circuits occurring at high temperatures.

1. Introduction

A battery, an energy storage device, is one of the most important parts of electrical gadgets, where electrochemical reactions occur and produce electricity [1, 2]. The battery business went through an evolution when Sony Corporation unveiled the first commercial LIB in 1991 [3]. An anode made of carbon, a cathode based on lithium compounds, an electrolyte, and a separator make up a typical LIB. The majority of studies into LIBs have focused on identifying the optimum electrode material in terms of specific energy, cycle life, capacity, and power, with little emphasis devoted to temperature control [4]. At high temperatures, LIBs performance degrades due to thermal runaway, aging, etc. Feng et al. [5] observed in their experiment that at high temperatures, the rates of deterioration of all LIB components increase. However, on the other hand, at low temperatures due to low kinematics, the battery performance is found limited [6]. Hence, it is very important to study the temperature effect on a lithium-ion battery and find an optimum safe operating temperature range. Complex electrochemical changes take place during the charging and discharging of a LIB with a significant amount of heat release. The performance, longevity, as well as safety of a Lithium-Ion battery, are affected by the operating or ambient temperature [7, 8]. In addition, temperature affects the ionic conductivities of electrodes and electrolytes [9]. The properties of electrolytes are affected when the battery is exposed to cold temperatures. At low temperatures, the internal resistance of the electrolyte rises due to its viscosity. As a result, the Lithium-ion diffusivity and the electrolyte's ionic conductivity, power, and capacity of the cell decrease [10–12]. The charge transfer resistance (Rct) is one of the most significant factors that also increases at low temperatures [6]. Zhang et al. interpreted in their experiment that it is more difficult to charge a drained Li-ion battery than it is to discharge a charged battery at a low temperature [6]. Petzl et al. [13] demonstrated that at low temperatures, lithium plating occurs. Lithium plating can penetrate separators and reduce capacity. These lithium dendrites, which are located on the surface of the negative electrode of LIBs, cause an internal short circuit [14]. However, high temperatures impair the performance of Lithium-ion batteries more than low temperatures. At room or standard operating temperature, electrochemical reactions and charge transfer produce heat inside the battery [15]. Irreversible processes such as heating due to mixing, polarization, enthalpy change, etc. are also responsible for generating heat. Xiao and Choe proposed a completely new heat generation formulation, which incorporates enthalpy heating and heat of mixing [15]. The Thermal Runway is another destructive phenomenon for a lithium-ion battery. It occurs when the heat formed inside a battery surpasses the quantity of heat released to its surroundings [16]. In Figure 1 thermal runaway process of a LIBs cell is illustrated. At high temperatures, exothermic

Appendix-IV

Back

Review

From Lithium-Ion to Sodium-Ion Batteries for Sustainable Energy Storage: A Comprehensive Review on Recent Research Advancements and Perspectives

Konok Chandra Bhowmik, Prof. Dr. Md. Arafat Rahman, Prof. Dr. Md. Muktadir Billah, Aoyon Paul

First published: 20 November 2024
https://doi.org/10.1002/tcr.202400176

Abstract

A significant turning point in the search for environmentally friendly energy storage options is the switch from lithium-ion to sodium-ion batteries. This review highlights the potential of sodium-ion battery (NIB) technology to address the environmental and financial issues related to lithium-ion systems by thoroughly examining recent developments in NIB technology. It is noted that sodium is more abundant and less expensive than lithium, NIBs have several benefits that could drastically lower the total cost of energy storage systems. In addition, this study examines new findings in important fields including electrolyte compositions, electrode materials, and battery performances of lithium-ion batteries (LIBs) and NIBs. The article highlights advancements in anode and cathode materials, with a focus on improving energy density, cycle stability, and rate capability of both LIBs and NIBs. The review also covers the advances made in comprehending the electrochemical mechanisms and special difficulties associated with NIBs, such as material degradation and sodium ion diffusion. Future research directions are discussed, with an emphasis on enhancing the scalability and commercial viability of sodium-ion technology over lithium on Electric Grid. Considering sustainability objectives and the integration of renewable energy sources, the review's assessment of sodium-ion batteries' possible effects on the future state of energy storage is included in its conclusion.

Conflict of Interests

The authors declare that there are no conflicts of interest.

References